Journal of Structural Geology 91 (2016) 177–194

Contents lists available at ScienceDirect

Journal of Structural Geology

journal homepage: www.elsevier.com/locate/jsg

Fault-zone structure and weakening processes in basin-scale reverse faults: The Moonlight Fault Zone, South Island, New Zealand

S. Alder, S.A.F. Smith*, J.M. Scott

Department of Geology, University of Otago, PO Box 56, 9054 Dunedin, New Zealand

ARTICLE INFO

Article history:
Received 12 April 2016
Received in revised form
8 August 2016
Accepted 4 September 2016
Available online 7 September 2016

Keywords:
Basin inversion
Reverse fault
Fault reactivation
Fault-zone structure
Fault zone weakening
Pseudotachylytes
Foliated cataclasite
Phyllosilicates
Mechanical anisotropy

ABSTRACT

The >200 km long Moonlight Fault Zone (MFZ) in southern New Zealand was an Oligocene basin-bounding normal fault zone that reactivated in the Miocene as a high-angle reverse fault (present dip angle 65°–75°). Regional exhumation in the last c. 5 Ma has resulted in deep exposures of the MFZ that present an opportunity to study the structure and deformation processes that were active in a basin-scale reverse fault at basement depths. Syn-rift sediments are preserved only as thin fault-bound slivers. The hanging wall and footwall of the MFZ are mainly greenschist facies quartzofeldspathic schists that have a steeply-dipping (55°–75°) foliation subparallel to the main fault trace. In more fissile lithologies (e.g. greyschists), hanging-wall deformation occurred by the development of foliation-parallel breccia layers up to a few centimetres thick. Greyschists in the footwall deformed mainly by folding and formation of tabular, foliation-parallel breccias up to 1 m wide. Where the hanging-wall contains more competent lithologies (e.g. greenschist facies metabasite) it is laced with networks of pseudotachylyte that formed parallel to the host rock foliation in a damage zone extending up to 500 m from the main fault trace. The fault core contains an up to 20 m thick sequence of breccias, cataclasites and foliated cataclasites preserving evidence for the progressive development of interconnected networks of (partly authigenic) chlorite and muscovite. Deformation in the fault core occurred by cataclasis of quartz and albite, frictional sliding of chlorite and muscovite grains, and dissolution-precipitation. Combined with published friction and permeability data, our observations suggest that: 1) host rock lithology and anisotropy were the primary controls on the structure of the MFZ at basement depths and 2) high-angle reverse slip was facilitated by the low frictional strength of fault core materials. Restriction of pseudotachylyte networks to the hanging-wall of the MFZ further suggests that the wide, phyllosilicate-rich fault core acted as an efficient hydrological barrier, resulting in a relatively hydrous footwall and fault core but a relatively dry hanging-wall.

1. Introduction

Large normal faults are frequently reactivated as high-angle reverse faults during compressional basin inversion (Fig. 1) (e.g. Turner and Williams, 2004). Reactivation and slip along high-angle reverse faults occurs in many cases within a regional stress field characterized by a sub-horizontal maximum principal stress (σ_1) (e.g. Sibson, 1990; Sibson, 2007). It follows that slip along high-angle reverse faults —as in the case of many low-angle normal faults and some strike-slip faults— must be facilitated by one or more fault weakening mechanisms that allow large displacements to accumulate in preference to the formation or reactivation of more optimally-oriented faults.

Due to the fact that inversion-related structures (e.g. hanging-wall antiforms) commonly form traps for hydrocarbons in petroleum reservoirs (e.g.Harding and Lowell, 1979; Doré and Lundin, 1996), much research on compressional basin inversion has focussed on the analysis of structural and stratigraphic geometries derived from seismic reflection profiling and regional-scale field analysis. These techniques have revealed a great deal of information on the kinematic development of inverted basins (e.g.Fraser and Gawthorpe, 1990; Bishop and Buchanan, 1995; Ghisetti and Sibson, 2006; Mescua and Giambiagi, 2012; Reilly et al., 2015). Analogue modeling of positive inversion has also been successful in replicating many of the structures that characterize natural examples, and has yielded additional insights in to the evolution of

* Corresponding author.
E-mail address: steven.smith@otago.ac.nz (S.A.F. Smith).

http://dx.doi.org/10.1016/j.jsg.2016.09.001
0191-8141/

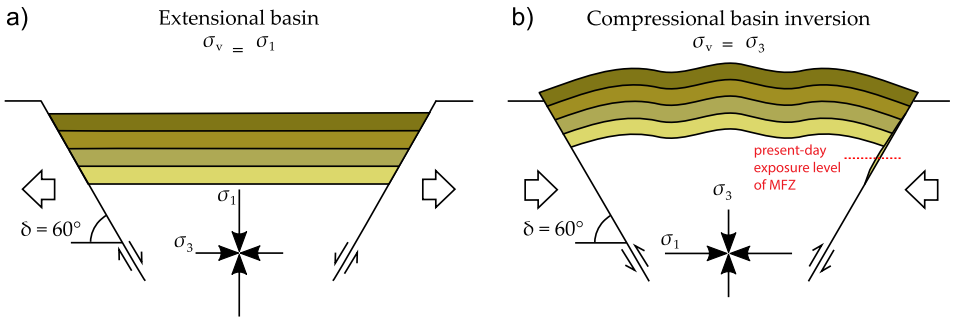

Fig. 1. Cartoon, modified from Sibson (2009), illustrating ideal a) coaxial extension and b) compressional inversion of a sedimentary basin bound by faults dipping at 60°. The present-day exposure level along the Moonlight Fault Zone is shown schematically in part b. In studied outcrops, basement rocks are present in both hanging wall and footwall, and syn-rift sediments are only preserved along the Moonlight Fault Zone as small fault-bound lenses and slivers.

inversion-related fault systems (e.g. McClay, 1995).

Prevailing mechanical models for high-angle reverse faulting emphasize the effects of high pore fluid pressure as a weakening mechanism to explain steep reverse slip (e.g. Sibson, 1995; Ghisetti and Sibson, 2012). Such models are supported by a range of geophysical data (e.g. bright-spot S-wave reflectors, seismic low-velocity zones, Vp/Vs ratios) indicating the presence of anomalously high fluid pressures in the source regions of several recent high-angle reverse fault ruptures, including in NE Honshu (Sibson, 2009). Additionally, field observations from relatively low-displacement reverse faults in areas of Au-mineralization show the presence of fault-hosted vein networks that are consistent with repeated attainment of supra-lithostatic fluid pressures at the time of steep reverse faulting (e.g.Sibson et al., 1988; Cox, 1995). However, many questions remain concerning the structure and physical properties of large-displacement (basin-scale) reverse faults, particularly in basement rocks (Fig. 1). Other possible weakening mechanisms that could promote nucleation and slip of high-angle reverse faults in the brittle crust include: (1) a range of mineralogical weakening processes (e.g. Wintsch et al., 1995a; Jefferies et al., 2006b; Smith and Faulkner, 2010), including the preferential reactivation of relatively weak planes in mechanically anisotropic rocks (Collettini et al., 2009; Massironi et al., 2011; Bistacchi et al., 2012); and (2) rotation of the principal stress axes within and surrounding the fault zone (Rice, 1992; Faulkner et al., 2006).

To further our understanding of the mechanics of positive inversion, this paper presents results from a field investigation of the Moonlight Fault Zone (MFZ) in the South Island of New Zealand. The MFZ was active in the Oligocene as a basin-scale normal fault zone. In the Miocene, the fault was reactivated during regional compressional inversion associated with uplift and exhumation of the Southern Alps mountain range (Norris et al., 1978). Reverse displacements on the MFZ were sufficiently large that syn-rift sediments are no longer preserved in the hanging-wall but only locally as small fault-bound slivers (Fig. 1b). Positive inversion continues in the South Island of New Zealand today, including in the Otago reverse-fault province (Litchfield, 2001) and the NW South Island reverse-fault province (Ghisetti and Sibson, 2006; Ghisetti et al., 2016), the latter hosting two of the largest historical earthquakes in New Zealand (1929 Buller M_S 7.8 and 1968 Inangahua M_S 7.4). Regional exhumation in the last c. 5 Ma has resulted in deep exposures of the MFZ that present a rare opportunity to investigate the structure and deformation processes that were active in a basin-scale reverse fault at basement depths.

2. Methodology

Observations and measurements of the structure and fault rock assemblages in the MFZ were made in five creek sections spread along a strike length of c. 70 km between the Matukituki Valley in the north and Twelve Mile Creek in the south (Fig. 2). Polished thin sections were prepared from oriented samples of the main fault rocks in the hanging-wall, fault core and footwall. Sections were cut perpendicular to host rock or fault rock foliations and parallel to lineations. Microstructural observations were carried out using a transmitted-light microscope and a Zeiss Sigma VP Field-Emission Scanning Electron Microscope (SEM; in the Otago Centre for Electron Microscopy, University of Otago) operating in backscattered mode (acquisition conditions: accelerating voltage 15 kV, working distance 6–8.5 mm). Energy-dispersive X-ray Spectroscopy (EDS) on the SEM was used to produce element maps.

Two phyllosilicate-rich fault rock samples from Matukituki Valley were analyzed with quantitative powder X-ray diffraction (XRD). Approximately 1.5 g of the samples were ground for 10 min in a micronizing mill under ethanol. The resulting slurries were oven dried at 60 °C then thoroughly mixed in an agate mortar and pestle before being lightly back pressed into stainless steel sample holders. Particle size separation was completed by dispersing approximately 8 g of the samples using a 1 wt% sodium hexametaphosphate – 1 wt% sodium carbonate solution. From this dispersion the <2 μm fraction was collected by repeated ultrasonification and centrifugation. XRD patterns were recorded with a PANalytical X'Pert Pro Multi-purpose Diffractometer using Fe filtered Co Kα radiation, automatic divergence slit, 2° anti-scatter slit and fast X'Celerator Si strip detector. Bulk diffraction patterns were recorded from 4 to 80° (3–33° for the oriented samples) in steps of 0.017° 2 theta with a 0.5 s counting time per step for an overall counting time of approximately 35 min. Qualitative analysis was performed on the XRD data using in-house XPLOT and HighScore Plus (from PANalytical) search/match software. Quantitative analysis was performed using the commercial package TOPAS from Bruker. Results normalized to 100% are listed in Table 1, and hence do not include estimates of unidentified or amorphous phases.

3. Geologic setting

3.1. Regional geology

Basement rocks of the South Island are broadly divided into the Western and Eastern Provinces (Fig. 2a), which both comprise multiple tectonostratigraphic terranes (e.g.Mortimer et al., 2002). The Western Province is made of Carboniferous to Early Paleozoic arc and sedimentary rocks that have been invaded by Paleozoic to Cretaceous plutons. It is separated from the fore-arc, back-arc and ophiolitic accretionary terranes of the Eastern Province by a

variably tectonised magmatic belt known as the Median Batholith (Mortimer et al., 1999; Scott, 2013).

The MFZ is part of the Eastern Province (Fig. 2b) and occurs within the Otago Schist, a metamorphic belt composed of rocks from the Caples Terrane, Rakaia Terrane and the Aspiring Terrane (Fig. 2c). These dominantly quartzofeldspathic terranes were amalgamated during Jurassic – Cretaceous orogenesis and preserve regional-scale isoclinal folds and large nappe structures (Craw, 1985). Metamorphic facies vary across the Otago Schist, ranging from prehnite - pumpellyite facies along the flanks of the medial antiform to upper greenschist facies in the centre (Mortimer, 2000) (Fig. 2b). The highest grade assemblages (garnet-biotite-albite zone greenschist) experienced conditions of 8–10 kbar and 350–400 °C (Mortimer, 2000).

3.2. The Moonlight Fault Zone

The MFZ was first recognized at Bobs Cove on the shores of Lake Wakatipu by Hacket (1864), where it is marked by a discontinuous thin sliver of Oligocene calcareous sediments known as the Bobs Cove Beds (Fig. 2c). Other isolated outcrops of Bobs Cove Beds occur along the MFZ north and south of Lake Wakatipu (McKay, 1881; Park, 1909; Hutton, 1939; Grindley, 1963; Barry, 1966; Turnbull, 1969). The MFZ was traced by Rattenbury et al. (2010) northwards towards the Alpine Fault (Fig. 2b) and has a total strike length of at least 200 km. On the basis of fieldwork, petrographic observations and palaeontological studies, Turnbull et al. (1975) suggested the following tectonic history for the MFZ:

1) A phase of pre-Early Oligocene strike-slip movement that produced a c. 1 km wide zone of deformation and kink folding in the schists surrounding the MFZ. From observations of the contact between the Dun Mountain Ophiolite Belt and Caples Terrane to the south of Lake Wakatipu (Norris et al., 1978), finite lateral offset during this phase is estimated to be < 1–2 km.
2) An Early Oligocene phase of normal faulting that correlates with regional extension and subsidence. Regional extension during this time occurred across much of the South Island and generated rapidly-subsiding, fault-controlled sedimentary basins (Turnbull et al., 1975; Norris et al., 1978). Norris et al. (1978) suggested that the MFZ initiated during the Early Oligocene as one of the basin-bounding normal fault zones down-throwing basement schist to the west and allowing for deposition of the Bobs Cove Beds. Some of the sediments that form the Bobs Cove Beds were derived from the upthrown block of schist in the footwall of the MFZ (Turnbull et al., 1975).
3) A Miocene or younger phase of high-angle reverse faulting as much of the South Island underwent broadly NW-SE directed compression as a result of oblique convergence along the Australian – Pacific plate boundary (Norris et al., 1990b). This phase of reactivation caused dismemberment and infaulting of the Bobs Cove Beds sediments, which are now preserved as relatively small lenses and slivers in the footwall of the main trace of the MFZ (Figs. 1, 2c and 3). Reverse faulting also resulted in the formation of broad regional-scale folds including the Earnslaw Synform and Shotover Antiform (Turnbull et al., 1975; Norris et al., 1978; Craw, 1985) (Fig. 2c). In close proximity to the MFZ, belts of tightly-spaced chevron folds and kink bands formed in the schists (Barry, 1966; Craw, 1985).

Based on a study of conjugate kink bands adjacent to the MFZ, Barry (1966) inferred that the maximum principal stress (σ_1) at the time of reverse faulting plunged shallowly (<10°) to the ESE, at large angles (>70°) to the MFZ (Fig. 2c). This estimate of paleo-σ_1 is similar to the present day regional orientation of σ_1 in Otago derived from studies of microseismicity, which infer a subhorizontal σ_1 trending between c. 110°–120° (Scholz et al., 1973; Norris and Carter, 1982; Reyners et al., 1983; Townend et al., 2012; Warren-Smith et al., 2015).

4. Structure and kinematics of the Moonlight Fault zone

4.1. Matukituki Valley

4.1.1. Host rocks

The MFZ in the Matukituki Valley has juxtaposed strongly foliated greenschist in the hanging-wall against folded greyschist in the footwall (Fig. 3a). At distances of tens to several hundreds of metres from the main fault trace, the greenschist has a moderately NW-dipping foliation (mean 025/54W) and NW-plunging mineral stretching lineation (Figs. 3a and 4a). The dip of the foliation progressively increases to become subparallel to the steeply west-dipping main fault trace (Figs. 3a and 4b). The hanging-wall greenschists are typically light grey-green and contain dark grey phyllosilicate-rich bands (Fig. 5a). The mineralogy (determined from optical and SEM observations and XRD) consists of chlorite, epidote, albite and titanite with minor stilpnomelane, actinolite, calcite, quartz, biotite, apatite and chalcopyrite.

The footwall consists of greyschist (Fig. 3a) made of >1 mm thick segregations of dark grey to pale green phyllosilicate-rich layers and white quartz-rich layers. The mineralogy consists of chlorite, quartz, muscovite, albite and calcite with minor epidote, titanite, clinozoisite and rutile. The greyschist is strongly foliated and contains tight (interlimb angle ave. 65°), centimeter-scale chevron folds that plunge shallowly to the south (Figs. 3a, 4c and 5b).

4.1.2. Fault-related deformation

The hanging-wall greenschists are laced with pseudotachylytes, which are overprinted by small cataclasite-bearing faults (Fig. 3a). Pseudotachylyte veins are mainly subparallel to the host rock foliation (Figs. 4d and 5c), whereas the cataclasite-bearing faults crosscut the foliation and pseudotachylyte veins (Figs. 4d and 5d). The small faults contain up to 10 cm of incohesive cataclasite and accommodate up to tens of centimetres of apparent slip. Offset markers and generally west-plunging lineations associated with the cataclasite-bearing faults indicate top-to-the-east reverse movements (Fig. 4d).

In the footwall greyschists, a c. 10 m wide zone of brecciation occurs adjacent to the main trace of the MFZ (Fig. 3a). The breccias evolve progressively to cataclasites and foliated cataclasites (Fig. 3a). This fault rock sequence, and the hanging-wall pseudotachylyte networks, are described in detail in section 6.

4.2. Stony Creek

4.2.1. Host rocks

In Stony Creek, the zone of deformation associated with the MFZ exceeds 1 km in width. Greenschist in the hanging-wall is juxtaposed against a thin (<10 m) sliver of Bobs Cove Beds in the footwall, which is turn is found in faulted contact with footwall greyschist (Fig. 3b). Foliation in the greenschist dips steeply to the west (mean - 001/67W), subparallel to the main trace of the MFZ (Fig. 4e). The Bobs Cove Beds are composed here of well-indurated sandstones with occasional quartz pebble beds up to 20 cm thick that lie subparallel to the main trace of the MFZ (Fig. 3b). The footwall greyschist is light grey with discontinuous quartz and albite layers up to 3 cm thick. It is highly fissile and well foliated with irregular kink bands and chevron folds present at least several hundred metres from the main fault trace. Adjacent to the main fault trace, the footwall foliation dips steeply to the west. Further

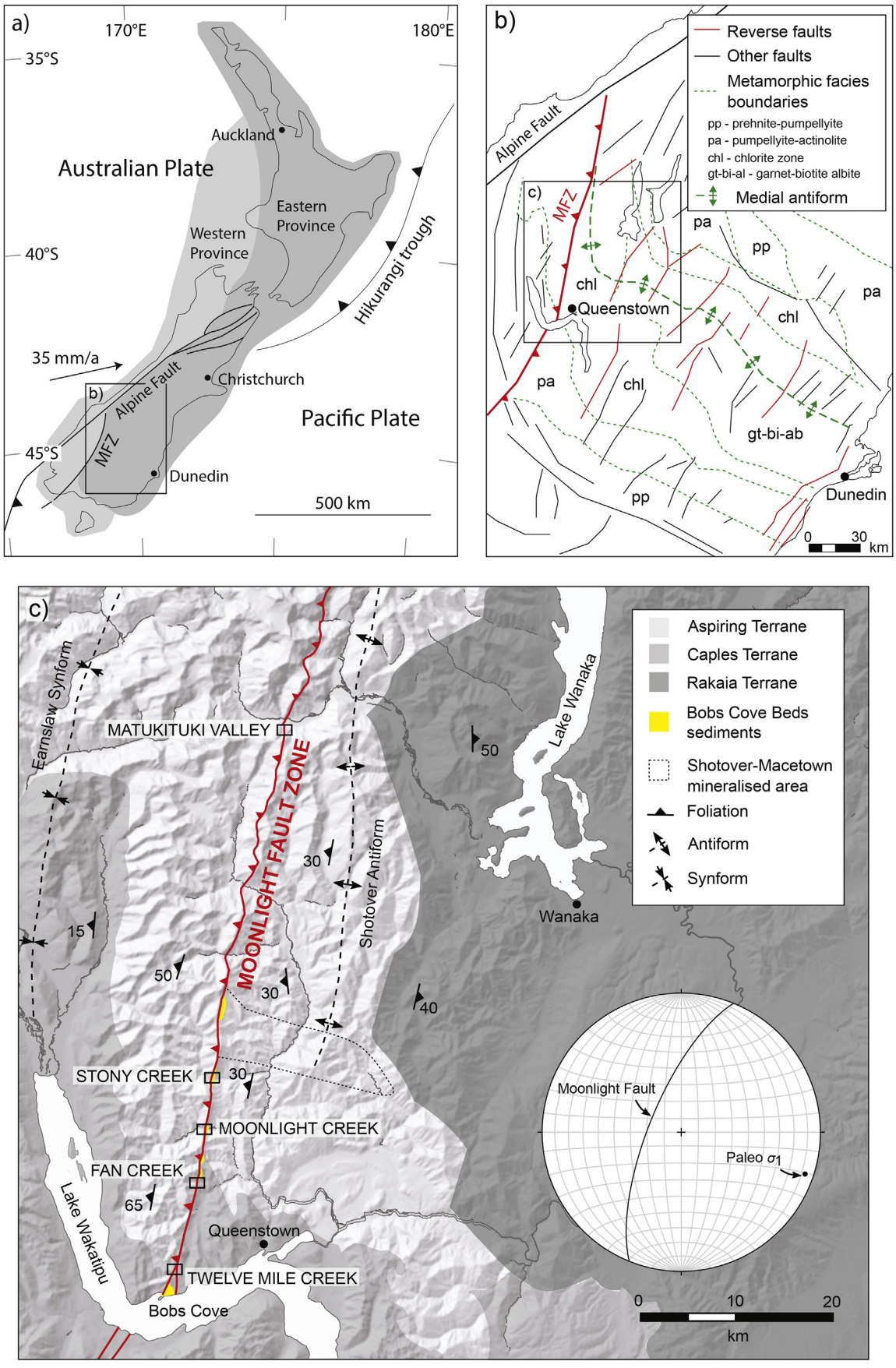
a)
170°E
180°E
35°S
40°S
45°S
Auckland
Australian Plate
Eastern Province
Western Province
Hikurangi trough
35 mm/a
Alpine Fault
b)
MFZ
Christchurch
Pacific Plate
Dunedin
500 km
b)
Reverse faults
Other faults
Metamorphic facies boundaries
pp - prehnite-pumpellyite
pa - pumpellyite-actinolite
chl - chlorite zone
gt-bi-al - garnet-biotite albite
Medial antiform
Alpine Fault
c)
MFZ
pa
pp
chl
Queenstown
gt-bi-ab
Dunedin
0 30 km
c)
Aspiring Terrane
Caples Terrane
Rakaia Terrane
Bobs Cove Beds sediments
Shotover-Macetown mineralised area
Foliation
Antiform
Synform
Earnslaw Synform
MATUKITUKI VALLEY
MOONLIGHT FAULT ZONE
Shotover Antiform
Lake Wanaka
Wanaka
STONY CREEK
MOONLIGHT CREEK
FAN CREEK
Lake Wakatipu
Queenstown
TWELVE MILE CREEK
Bobs Cove
Moonlight Fault
Paleo σ1
0 10 20 km

east the foliation defines a large antiform-synform pair with wavelengths on the order of a few hundred metres (Fig. 3b; Fig. 4f).

4.2.2. Fault-related deformation

The main trace of the MFZ in Stony Creek is a well-defined, continuous and relatively planar feature marked by 35–45 cm of foliated green and black gouge (Fig. 5e). The green and black gouges are in places separated by a discrete slip surface that dips steeply to the west (020/74W; Fig. 4e). As in the Matukituki Valley, deformation in hanging-wall greenschist is dominated by foliation-parallel pseudotachylytes and cataclasite-bearing faults that crosscut the pseudotachylytes (Figs. 3b and 4e). The footwall sedimentary package is host to discrete shears of variable orientation (Figs. 3b and 4g). The shears disrupt and offset the margins of the green and black gouge layers but were not observed to offset the slip surface separating the gouge layers (Fig. 5e). The base of the sedimentary package is marked by a series of stepped fault surfaces (Fig. 3b). In the easterly dipping limb of the footwall anticline, c. 200 m from the main fault trace, an up to 1 m wide well-indurated breccia crosscuts the footwall foliation and strikes NNW with a dip of 44° NE (Figs. 3b and 4f).

4.3. Moonlight Creek

4.3.1. Host rocks

In Moonlight Creek, fissile greyschist and quartzofeldspathic gneiss in the hanging-wall are juxtaposed against Bobs Cove Beds that lie unconformably on greyschist in the footwall (Fig. 3c). The hanging-wall quartzofeldspathic gneiss has white and grey segregations that define a steeply west-dipping foliation (182/75W; Figs. 3c and 4h). Adjacent to the main fault trace a c. 10 m wide zone of heavily sheared fissile greyschist is present in the hanging-wall (Fig. 3c). The foliation in the sheared greyschist dips steeply to the west (007/72W) subparallel to the main trace of the MFZ (Fig. 4h). In the footwall, a c. 30 m wide package of well-indurated, light grey sandstone of the Bobs Cove Beds is present (Figs. 3c and 5f). Bedding strikes NE-SW and dips steeply NW (037/66W; Fig. 4i). The basal (eastern) contact of the sedimentary package lies unconformably on footwall greyschists, indicating a westerly younging direction in the sediments. The footwall greyschist contains a steeply west-dipping foliation (Figs. 3c and 4i) and is typically light grey and fissile with occasional more massive greenschist layers up to 30 cm wide.

4.3.2. Fault-related deformation

The main trace of the MFZ in Moonlight Creek is marked by a prominent 1–2 m wide gully containing cohesive black cataclasites and ultracataclasites up to 1 m thick that define the top surface of the Bobs Cove Beds (037/66 W; Fig. 4j). Above the cataclasites, a c. 35 cm-1 m wide zone contains intimately mixed, incohesive green and black gouges (Fig. 3c). Deformation in the hanging-wall is dominated by foliation-parallel pseudotachylytes and cataclasites (Figs. 3c and 4j) that occupy a zone extending at least 100 m from the main fault trace (Fig 3c). These are crosscut by younger, dark-grey to black shears and small cataclasite-bearing faults (Figs. 3c and 4j). Deformation in the footwall Bobs Cove Beds is represented by stylolites with variable orientations. The footwall greyschist is deformed most intensely in the 15 m below the unconformity (Fig. 3c). In this area, the greyschist hosts numerous east-verging S folds and a series of foliation-parallel breccia layers up to 1 m wide (Figs. 3c and 4k). The breccias contain fault surfaces with slickenlines that plunge steeply NW (Fig. 4k).

One thick breccia layer was found in footwall greyschist c. 750 m from the main trace of the Moonlight Fault, lying subparallel to the footwall foliation (Figs. 4k and 6a). The western margin of the breccia is marked by a prominent fault surface that strikes north and dips steeply to the west (177/73 W), subparallel to the surrounding foliation (Fig. 6c). A R_1-type Riedel shear band (Logan et al., 1979) lies at c. 25° to the margin of the breccia (Fig. 6b). On the assumption that the slip vector in the breccia was perpendicular to the intersection of the main fault plane and the R_1-shear band, the shear direction plunges moderately SSW (46/196; Fig. 6c). Asymmetric folds within the breccia and kink bands in the surrounding greyschist indicate that movement was top-to-the-NNE.

Table 1
Results of quantitative X-Ray Diffraction analysis on the bulk and <2 μm fractions of the footwall- and hanging-wall-derived foliated cataclasites from the core of the Moonlight Fault in the Matukituki Valley.

	Mineral weight percent (wt%)				
	Quartz	Albite	Chlorite	Muscovite	Titanite
Bulk					
Footwall-derived	23.4	14.7	7	54.9	
Hanging wall-derived	13.1	9.8	71.7		5.4
<2 μm fraction					
Footwall derived	2.8	2.4	11.9	82.8	
Hanging wall-derived	1.9	0.7	96.2		1.2

4.4. Fan Creek

4.4.1. Host rocks

In Fan Creek, the MFZ juxtaposed greyschists and phyllites in the hanging-wall against Bobs Cove Beds (Fig. 3d) or Caples Terrane phyllites and schist in the footwall. The zone of fault-related deformation is >600 m wide. The hanging-wall consists of black phyllite with a strong foliation that strikes NS and dips steeply west (mean - 173/65W; Fig. 4l), which rotates to strike NE-SW within 20 m of the main fault trace (Fig. 4l). The package of Bobs Cove Beds in the footwall immediately north of Fan Creek has a maximum thickness of c. 75 m and includes a basal conglomerate and overlying yellow sandstones with quartz beds and thin mud beds. The bedding in the sedimentary package is locally overturned, dipping steeply south-east (mean of 054/83SE; Fig. 4m).

The schist in the footwall is made up of three types, from west to east: 1) a c. 10 m thick weakly foliated green phyllite that is faulted along its eastern margin against 2) a brecciated schist that is faulted along its eastern margin against 3) a light-green schist with a steep south-easterly dip (mean - 033/78E; Fig. 4m). The eastward dipping foliation in the schist is a local feature, with the regional footwall foliation dipping steeply to the west, subparallel to the MFZ (Barber and Craw, 2002).

4.4.2. Fault-related deformation

The main trace of the MFZ in Fan Creek dips steeply to the west (178/77W; Fig. 4m). The fault consists of a 10 cm thick black foliated

Fig. 2. Tectonic overview of the Moonlight Fault Zone (MFZ). a) Regional setting of the study area relative to the Alpine Fault and the Western and Eastern Provinces in New Zealand. b) Map of main fault systems and metamorphic facies in the Otago area. c) Simplified geological map adapted from Rattenbury et al. (2010) showing the trace of the Moonlight Fault Zone, the boundary between the Rakaia, Aspiring and Caples Terranes, the location of the Bobs Cove Beds along the MFZ and the boundaries of the Shotover-Macetown mineralized area. Boxes show the locations of the five studied creek sections that are described from north to south in section 4. Equal area lower hemisphere projection shows inferred σ_1 at the time of steep reverse faulting from analysis of conjugate kink bands by Barry (1966). The great circle is a representative orientation of the main trace of the Moonlight Fault based on (Barry, 1966; Norris et al., 1978; Barber and Craw, 2002) and fieldwork presented here.

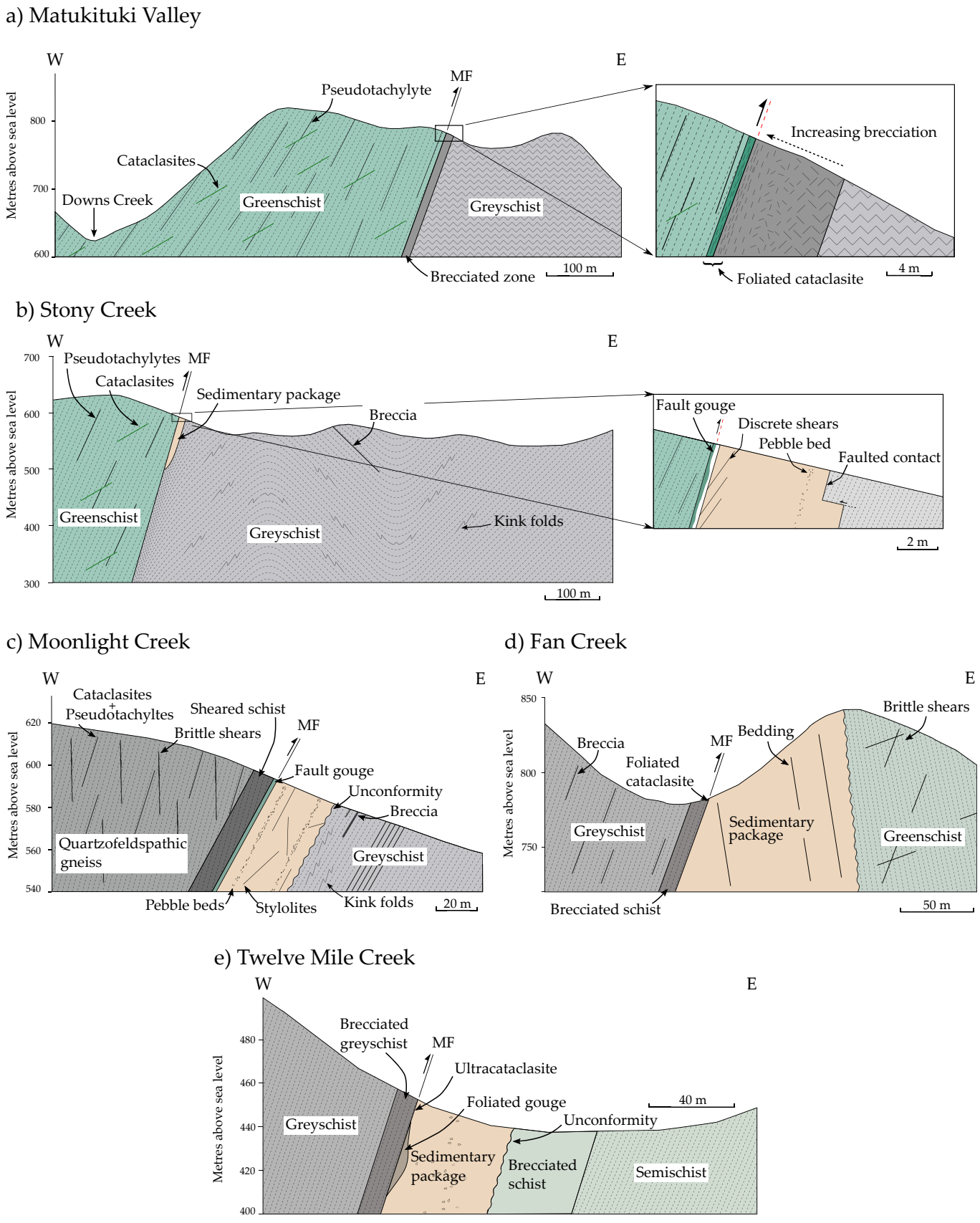

Fig. 3. Cross sections through the Moonlight Fault Zone in five creeks illustrating the orientations and structure of the main host rock fabrics and fault rock assemblages in the hanging-wall, fault core and footwall. Cross sections a-e are from north to south and locations are shown on Fig. 2c. MF, main trace of the Moonlight Fault Zone mapped in the field. Note the change in scale between cross sections. a) Matukituki Valley, b) Stony Creek, c) Moonlight Creek, d) Fan Creek, and, e) Twelve Mile Creek.

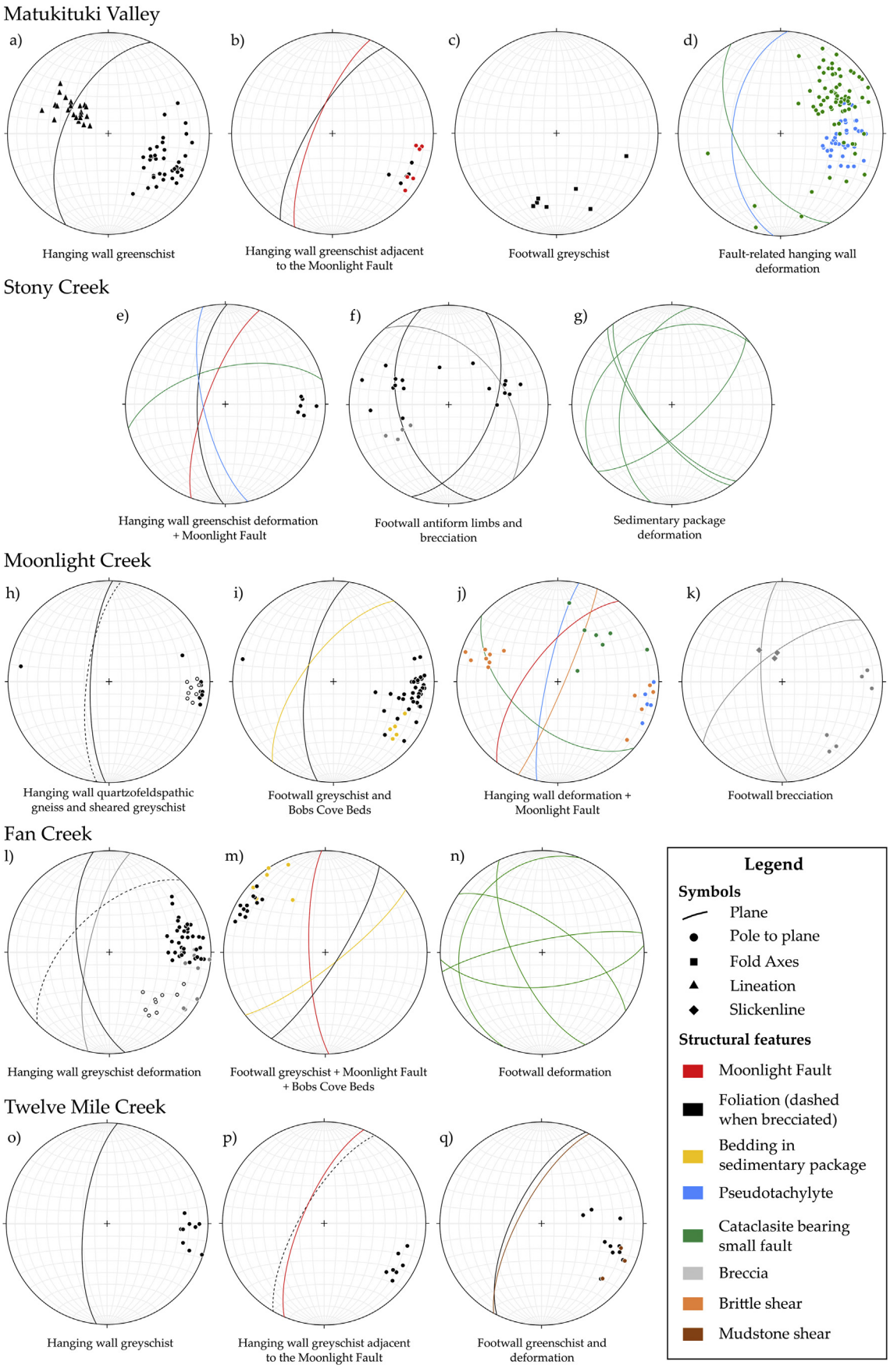

Fig. 4. Equal area lower hemisphere projections of host rock and fault-related deformation features associated with the MFZ.

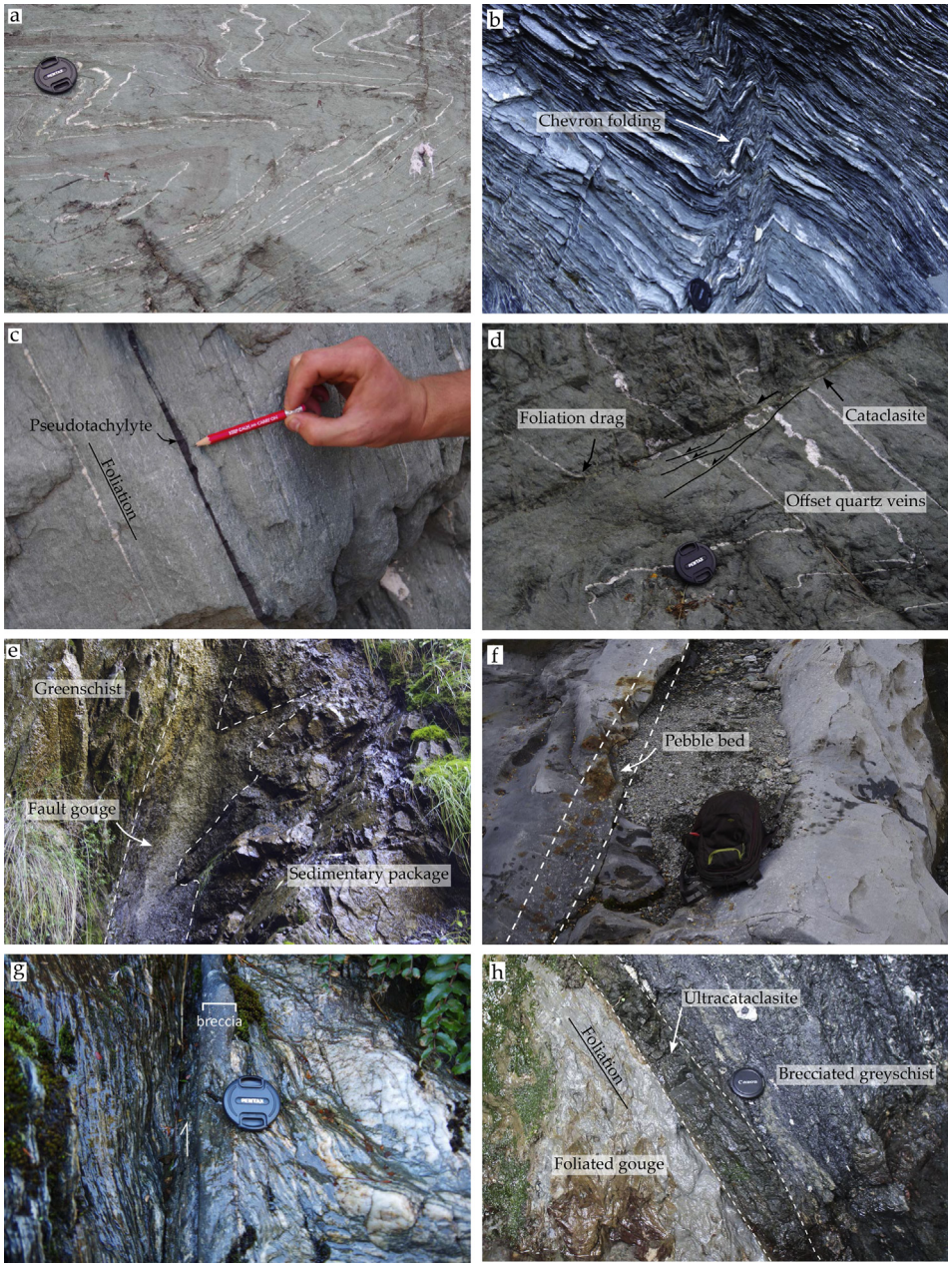

Fig. 5. Field photos of structures in the Moonlight Fault from the Matukituki Valley to Twelve Mile Creek. a-b) Photos of the hanging-wall greenschists (a) and the footwall greyschists with chevron folds (b) in the Matukituki Valley. c) Foliation parallel pseudotachylyte fault vein in the Matukituki Valley. d) Late-stage cataclasite offsetting features in the hanging-wall greenschists, Matukituki Valley. e) Green and black fault gouges within the core of the Moonlight Fault Zone in Stony Creek. Brittle shears in the sedimentary package enter the gouge but do not offset the slip surface separating green and black gouges. f) Photo of the sedimentary package in Moonlight Creek. Outlined is a steeply west-dipping pebble bed. g) Foliation parallel breccia in the hanging-wall of the Moonlight Fault Zone in Fan Creek. h) Core of the Moonlight Fault in Twelve Mile Creek. Brecciated greyschist in the hanging-wall contacts ultracataclasites which lie in contact with a foliated gouge likely derived from the Bobs Cove Beds sediments. (For interpretation of the references to colour in this figure legend, the reader is referred to the web version of this article.)

cataclasite at the schist-sediment contact, or a 30 cm thick incohesive red gouge layer at the schist-schist contact. The hanging-wall phyllite hosts numerous foliation-parallel breccias up to 10 cm thick (Figs. 4l and 5g). These breccias contain <2 mm wide clasts of host rock supported by a fine-grained matrix of quartz, albite, epidote, white mica and titanite that is cemented with calcite. Also present in the hanging-wall are kink folds and shear bands, which increase in frequency towards the main trace of the MFZ. Adjacent to the main fault trace, the hanging-wall phyllite is extensively brecciated (Fig. 3d). Within a few metres of the main fault trace, the brecciated phyllite is crosscut cut by quartz veins up to 30 cm thick, several of which taper upwards from the main fault trace into the hanging-wall. The footwall is host to late-stage, small cataclasite-bearing faults with an array of orientations (Fig. 4n).

4.5. Twelve Mile Creek

4.5.1. Host rocks

In Twelve Mile Creek, the MFZ juxtaposed Aspiring Terrane greyschists in the hanging-wall against a thin sliver of Bobs Cove Beds in the footwall that lie unconformably on low grade Caples Terrane semischist (Fig. 3e). Intact greyschist has a northerly

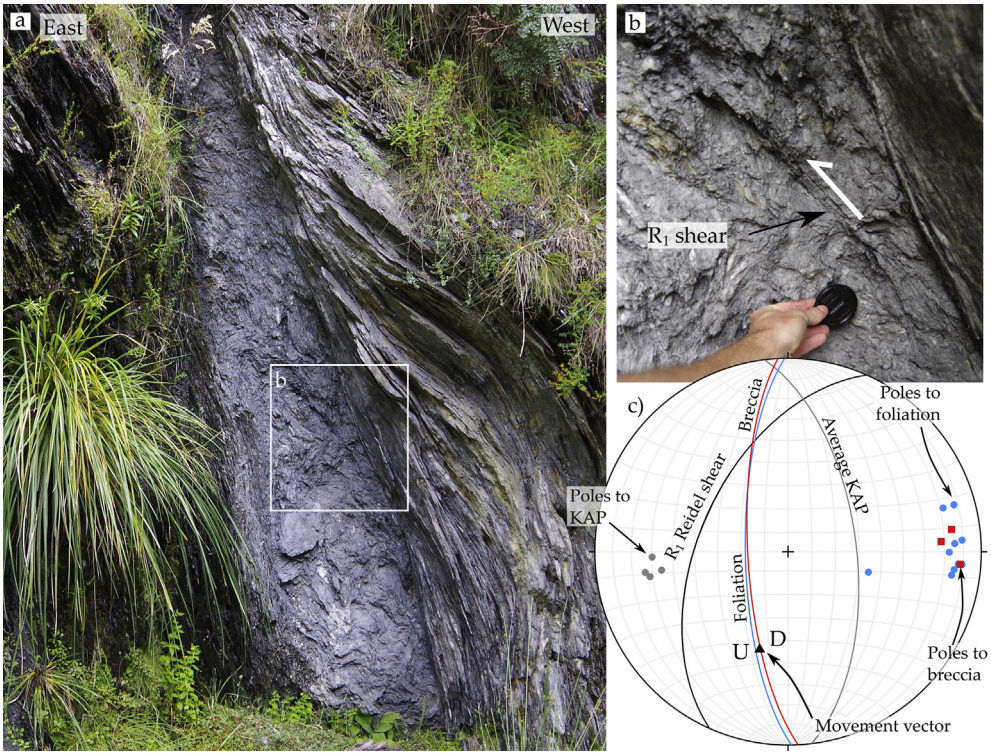

Fig. 6. Deformation in the footwall of the Moonlight Fault Zone in Moonlight Creek. a) An up to 1 m wide breccia layer c. 750 m from the main trace of the Moonlight Fault. The breccia lies subparallel to the surrounding greyschist foliation. b) R_1-type Reidel shear that is orientated at c. 25° to the upper breccia margin. c) Equal area lower hemisphere projection shows the orientation of the main breccia body (red; n = 3), foliation (blue; n = 10) and kink axial planes (KAP; n = 4) in the surrounding greyschist, and one R_1-type Reidel shear (black). Assuming the movement vector lies in the plane of the breccia layer and perpendicular to the intersection of the breccia and R_1-shear, this indicates top-to-NNE oblique reverse movements (combined with assymmetric folds adjacent to the breccia). (For interpretation of the references to colour in this figure legend, the reader is referred to the web version of this article.)

striking foliation that dips steeply to the west (006/71W; Fig. 4). The hanging-wall greyschist is brecciated at < 5 m from the main fault trace (Figs. 3e and 5h) and a foliation subparallel to the Moonlight Fault has developed (Fig. 4p).

In the footwall adjacent to the Moonlight Fault, a >40 m thick package of Bobs Cove Beds is present (Fig. 3e). These young to the west and consisting predominately of a matrix-supported conglomerate. The sediments lie unconformably upon a brecciated schist that contains fragments of low-grade schist (Fig. 3e), which in turn lies in contact with low-grade semi-schist of mainly psammitic composition (Fig. 3e). Psammitic layers in the semi-schist are light grey-green and contain a foliation that strikes N-NE and dips steeply to the west (026/67W; Fig. 4q).

4.5.2. Fault-related deformation

The main trace of the MFZ in Twelve Mile Creek is marked by a black, cohesive ultracataclasite (Fig. 5h) that commonly forms a resistant and relatively planar bench. The ultracataclasite strikes north and dips steeply to the west (023/72 W; Fig. 4p). Innaccessible slickenlines on the surface of the ultracataclasite bench were steeply plunging (rake >60°). In one location a foliated grey-green gouge layer up to c. 1 m thick, likely derived from the footwall sedimentary package, is present adjacent to the ultracataclasites (Fig. 5h). Within the footwall semischist, some of the mudstone layers host shear surfaces that are subparallel to the Moonlight Fault (Fig. 4q).

5. Synoptic view of the structure of the Moonlight Fault Zone

Although the structure and fault rock assemblages documented in section 4 vary along the strike of the MFZ, several general characteristics are apparent, summarized in Fig. 7:

Hanging-wall

1) The hanging-wall of the MFZ consists of competent greenschist and quartzofeldspathic gneiss or more fissile greyschist. All contain a steeply west-dipping foliation.
2) In greenschist and quartzofeldspathic gneiss, fault-related deformation is dominated by networks of steeply-dipping and foliation-parallel pseudotachylyte (section 6.1).
3) In fissile greyschists, fault-related deformation is dominated by foliation-parallel breccias.

Footwall

4) Footwall rocks are mainly folded and fissile greyschists with a steeply west-dipping foliation.
5) Fault-related deformation is expressed as thick breccia layers that are subparallel to foliation.
6) Where present, sediments of the Bobs Cove Beds lie in faulted or unconformable contact with footwall greyschists. Deformation in the Bobs Cove Beds occurs as small-displacement faults and stylolites with an array of orientations.

Main fault trace

7) Where fissile greyschists lie adjacent to the main trace of the MFZ they are brecciated in a zone up to 20 m wide. Towards the main fault trace, the breccias progressively evolve to cataclasite and foliated cataclasite or gouge (section 6.2).

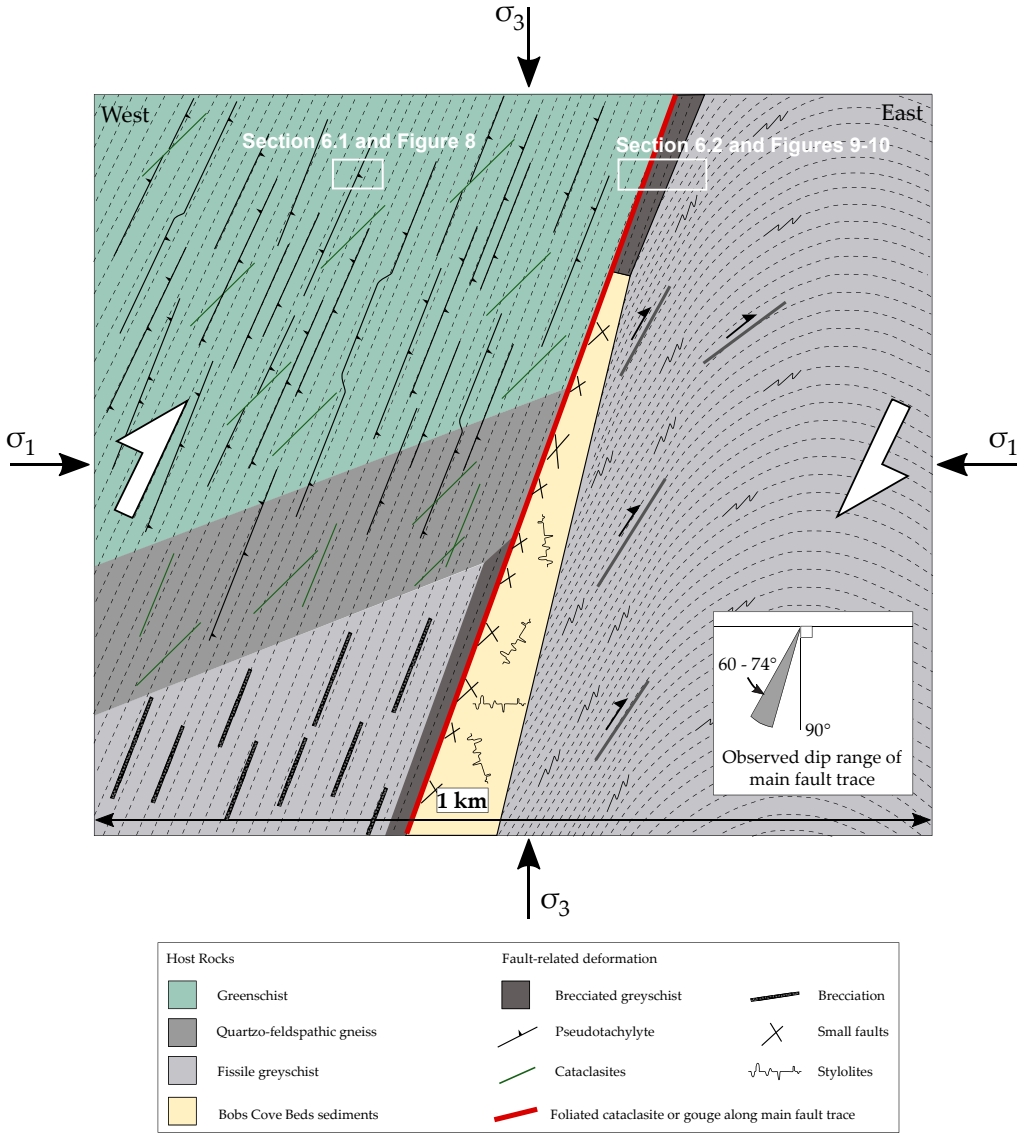

Fig. 7. Synoptic overview of the structure of the Moonlight Fault Zone. The total width of deformation related to reverse movements along the Moonlight Fault Zone is approximately 1 km. Inset shows the range of measured dip values of the main fault trace.

6. Microstructures and deformation processes in Moonlight Fault rocks

In this section, the microstructural characteristics of two of the dominant fault rock assemblages are described: the hanging-wall pseudotachylyte networks (section 6.1) and the breccia to foliated cataclasite sequence along the main fault trace. These observations are largely based on samples collected from the Matukituki Valley (Fig. 3a) where there is a particularly well-exposed section through the hanging-wall and fault core.

6.1. Hanging-wall pseudotachylyte networks

Pseudotachylyte fault veins (Sibson, 1975) in the MFZ could be traced for no more than c.15 m, although in some cases this was due to the limited lateral continuity of the outcrops. Most fault veins occur as discrete planar features (Fig. 8a–c) that on average lie subparallel to the steeply west-dipping greenschist foliation, although in detail often crosscut the foliation at low angles. The veins are aphanitic, dark grey-black and range in thickness from c. 200 μm to 7 mm, although most are <2 mm thick (Fig. 8b, c). Typically only one fault vein was observed, although in rare cases up to three parallel fault veins were linked by small melt pools and melt-filled fractures. Injection veins were observed infrequently to branch off fault veins at high angles (>60°) and range from 250 μm–4 cm in length and 300 μm - 3 mm at the widest point.

In two water-worn creek sections, the density of foliation-parallel pseudotachylyte fault veins was measured along transects perpendicular to the greenschist foliation. In Moonlight Creek a 21 m long transect revealed five foliation-parallel fault veins, with an average spacing of 4.6 m. In the Matukituki Valley a 2.6 m long transect revealed eight foliation-parallel fault veins with an average spacing of 0.23 m. Displacement on fault veins was difficult to determine due to a lack of suitable offset markers. General observation of markers on either side of fault veins indicates that displacements did not likely exceed a few tens of centimetres.

Foliation-parallel pseudotachylyte fault veins are linked in stepover regions by irregular fracture networks that cut across the

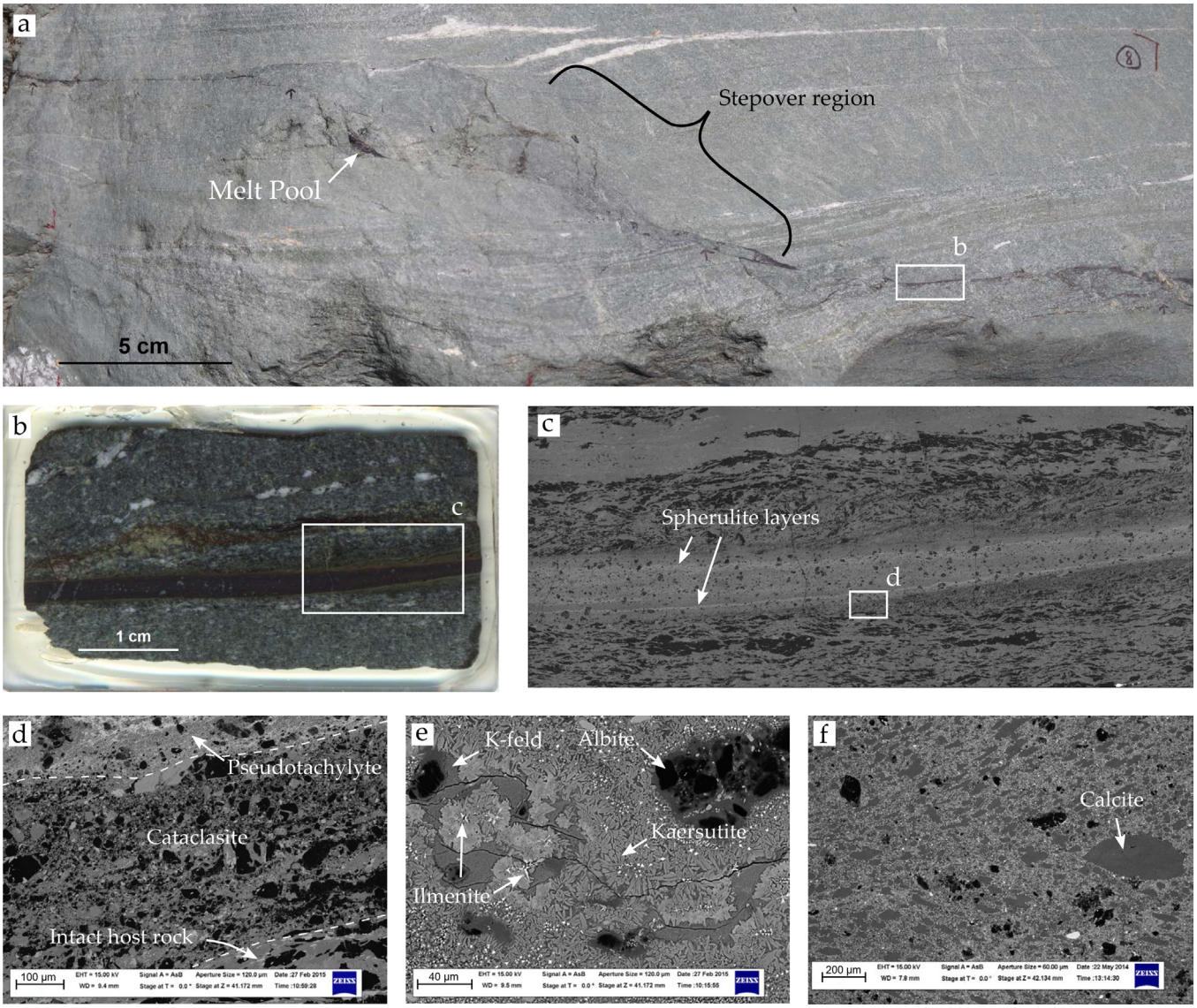

Fig. 8. Hanging-wall pseudotachylyte networks in the Matukituki Valley. Parts c-f are backscatter SEM images. a) Photo of foliation-parallel pseudotachylyte fault veins that are linked in a stepover region by a zone of pseudotachylyte breccia containing melt pools. b) Scanned thin section image of a foliation-parallel pseudotachylyte fault vein. Light green material along the margins of the fault vein is ultracataclasite. c) Foliation-parallel pseudotachylyte fault vein. Concentrations of spherulites define compositional and grain size bands that give the fault vein a layered appearance. d) Ultracataclasite adjacent to a pseudotachylyte vein margin indicating that cataclasis preceded frictional melting. e) Lithic albite grain breaking down to potassium feldspar. Kaersutite spherulites form around ilmenite microlites. f) Fault vein that hosts calcite-filled amygdules. The subparallel nature of the vesicle long axes defines flow paths within the fault vein. (For interpretation of the references to colour in this figure legend, the reader is referred to the web version of this article.)

greenschist foliation (Fig. 8a). These occur in zones up to 30 cm wide associated with brecciation of the host greenschist and formation of irregular melt pools (Fig. 8a).

Along the margins of fault veins, light-green ultracataclasites are commonly present (Fig. 8b–d). The ultracataclasites are <2 mm wide and commonly pinch out along the length of the vein. Strands of pseudotachylyte were found to occasionally branch into the ultracataclasites indicating that the ultracataclasites formed during an early stage of comminution.

The pseudotachylytes consist of lithic clasts - fragments of host greenschist that resisted melting - that lie within a matrix of optically resolvable grains that crystallised from melt (microlites) and/or a very fine cryptocrystalline matrix. Lithic fragments are predominately quartz and albite (Fig. 8e) with minor apatite, polycrystalline greenschist fragments and reworked ultracataclasite. The quartz and albite lithic grains are commonly 10–100 μm in size. Albite clasts are often fractured or completely disaggregated, contain melt embayments and have potassium feldspar rims (Fig. 8e). Quartz clasts occur in polycrystalline and monocrystalline forms, the former containing melt embayments which preferentially intrude along grain boundaries. The monocrystalline quartz clasts are intact and appear as rounded to subrounded spherical and elongate clasts, some of which show undulose extinction. Apatite occurs as grains typically <10 μm in size and rarely up to 20 μm. Reworked clasts of ultracataclasite, interpreted to form in the initial stages of pseudotachylyte formation (Spray, 1995) (Fig. 8d), show extensive melt embayments along grain boundaries.

The pseudotachylytes contain radial spherulites including Ti-rich amphibole (kaersutite) that sit in a potassium feldspar-rich matrix (Fig. 8e). Spherulite-rich bands define layering in the pseudotachylytes that is subparallel to fault vein margins (Fig. 8c).

Crystal size is variable between and within individual spherulites, but is typically 5–15 μm in length and 1–3 μm in width. Spherulites near the pseudotachylyte margin are generally smaller. The spherulites commonly form as elongate crystals at high angles to lithic albite clasts and ilmenite microlites (Fig. 8e).

Ilmenite microlites are most commonly granular in form (after Lin, 2008), although they also have a dendritic habit with crystals up to 20 μm long. Other newly grown microlite phases include very small (<2 μm) titanite grains that form in clusters, and iron oxide grains that are mainly <1 μm equant grains. The iron oxide grains are abundant in some pseudotachylyte veins such that they form seams that wrap around lithic clasts. Chlorite also occurs as small, randomly oriented laths up to 6 μm in length and 1–2 μm in width. Quantitative chemical analysis by EDS revealed that the cryptocrystalline matrices consisted of a phase with composition similar to either biotite or chlorite. XRD analysis of one pseudotachylyte sample also identified chlorite as a main phase.

A pseudotachylyte fault vein in the Matukituki Valley contains ellipsoidal calcite-filled amygdules (Fig. 8f). The amygdules reach up to 500 μm in length and 200 μm in width, although they are more commonly 10s of μm in length and 10–20 μm in width. The long axes of the amygdules are consistently aligned parallel or subparallel to the fault vein margins. Some amygdules have irregular shapes that reflects collapse before the precipitation of calcite.

6.2. Fault core breccias and cataclasites

The main trace of the MFZ in the Matukituki Valley – referred to below as the fault core - contains a sequence of breccias, cataclasites and foliated cataclasites in a zone up to 20 m wide. This sequence is preferentially developed in the fissile footwall greyschists (Figs. 7 and 9), whereas greenschists and well-cemented sedimentary rocks of the Bobs Cove Beds contain much narrower zones of localized faulting and brecciation. Fig. 9 shows samples collected at varying distances from the fault core in the Matukituki Valley.

6.2.1. 10 m in to the footwall

At a distance of c. 10 m from the fault core the footwall greyschist is relatively intact (Fig. 9a). Fold hinges and limbs are recognisable although the fold limbs are often cut and slightly disrupted by black shears. Clasts are clearly derived from the local greyschist host rock and have not experienced significant rotation.

6.2.2. 8 m in to the footwall

At a distance of c. 8 m from the fault core the greyschist fold hinges become increasingly disrupted to form a breccia (Fig. 9a). The breccia contains >60% clasts (at the optical microscope scale) up to a few centimetres in size. Some areas of the breccia contain clasts that are randomly oriented and cannot easily be related to nearby clasts, having experienced a significant amount of fracture and rotation.

6.2.3. 4 m in to the footwall

At a distance of c. 4 m from the fault core the breccia does not preserve any remnant host rock fabrics (Fig. 9a). Sub rounded clasts up to 2 cm in size are set in a very fine grained black matrix. Polycrystalline clasts are elongate parallel to the main trace of the Moonlight Fault and the matrix contains thin black seams that define a weak foliation subparallel to the Moonlight Fault.

6.2.4. 1-2 m in to the footwall

At a distance of c. 1–2 m from the fault core a foliated cataclasite is developed (Fig. 9a). The foliation is orientated subparallel to the main trace of the MFZ and is defined by the preferred alignment of the long axes of quartz and albite clasts derived from the host rock greyschist. The matrix represents >70% of the samples and contains dark seams up to 5 mm wide that define a foliation subparallel to the Moonlight Fault.

6.2.5. Foliated cataclasites in the fault core

Two types of foliated cataclasite are present in the fault core: 1) On the footwall side, a dark grey to black foliated cataclasite (labelled as B in Fig. 9a) represents a continuation of the progressively brecciated sequence described above; 2) on the hanging-wall side, a dark green foliated cataclasite (labelled as A in Fig. 9a) is derived from the hanging-wall greenschists (Fig. 9a). Both types of foliated cataclasite contain seams of fine-grained phyllosilicates up to 3 cm wide (Fig. 9b) that anastomose around clast-rich regions predominately composed of quartz and albite. The preferred orientation of clasts and seams define a foliation that lies subparallel to the Moonlight Fault (Fig. 9a).

Overall, rocks in the footwall of the Moonlight Fault show a textural transition towards the fault core that includes (Fig. 9a): 1) an increase in the degree of brecciation and cataclasis associated with a progressive decrease in grain size, 2) an increase in the total matrix proportion and a modal increase in the abundance of phyllosilicates, and 3) the progressive development of a fault-parallel foliation defined by the alignment of phyllosilicate phases and clasts.

6.3. Deformation mechanisms in the fault core

The footwall-derived foliated cataclasites in the fault core (Fig. 9a) contain muscovite, quartz, albite and chlorite (from XRD analysis, Table 1) with minor titanite and rutile (from optical microscope and SEM observations). The clast-rich domains consist largely of heavily fractured, polycrystalline quartz and albite clasts (Fig. 10a,b). The matrix is composed predominately (>80 wt%) of muscovite grains <2 μm in size as identified by quantitative XRD analysis (Fig. 10a,b; Table 1). Muscovite forms an interconnected network around quartz and albite clasts (Fig. 10b). Quartz and albite clasts often contain authigenic chlorite and muscovite overgrowths in “strain shadow” regions, giving them an elongate appearance (Fig. 10c), and chlorite is also present infilling fractures in quartz-albite clasts. Within the matrix, anastomosing seams preferentially developed subparallel to the steeply west dipping main fault (Figs. 9a and 10a). The seams truncate the top and bottom of quartz and albite clasts (Fig. 10d). SEM-EDS analysis indicates that the seams contain concentrations of iron (most likely in magnetite; Fig 10d) and titanium (most likely in rutile) and are therefore interpreted as dissolution seams (Fig. 10d).

The hanging-wall-derived foliated cataclasites in the fault core contain chlorite, quartz, albite and titanite (from XRD analysis, Table 1), as well as epidote, plagioclase, apatite and rutile (from optical microscope and SEM observations). Clast-rich domains form elongate fractured boudins up to 3 cm wide within a green chlorite-rich matrix that forms an anastomosing interconnected network (Figs. 9b and 10e). The matrix is dominated by chlorite (>96 wt% as identified by quantitative XRD analysis on the <2 μm fraction; Table 1) with minor quartz, albite and titanite (Table 1). Chlorite grains in the matrix are up to 5 μm wide and also form in tails around quartz and albite clasts. Epidote forms very fine grained masses or small (<0.2 mm) elongate crystals which align parallel or subparallel to the foliation (Fig. 10e). Quartz and albite clasts are commonly fractured at high angles to the clast long axis, with fractures infilled by chlorite (Fig. 10e, f). Albite clasts also protrude into one another across irregular dissolution seams enriched in opaque minerals (identified as magnetite by SEM-EDS analysis; Fig. 10f).

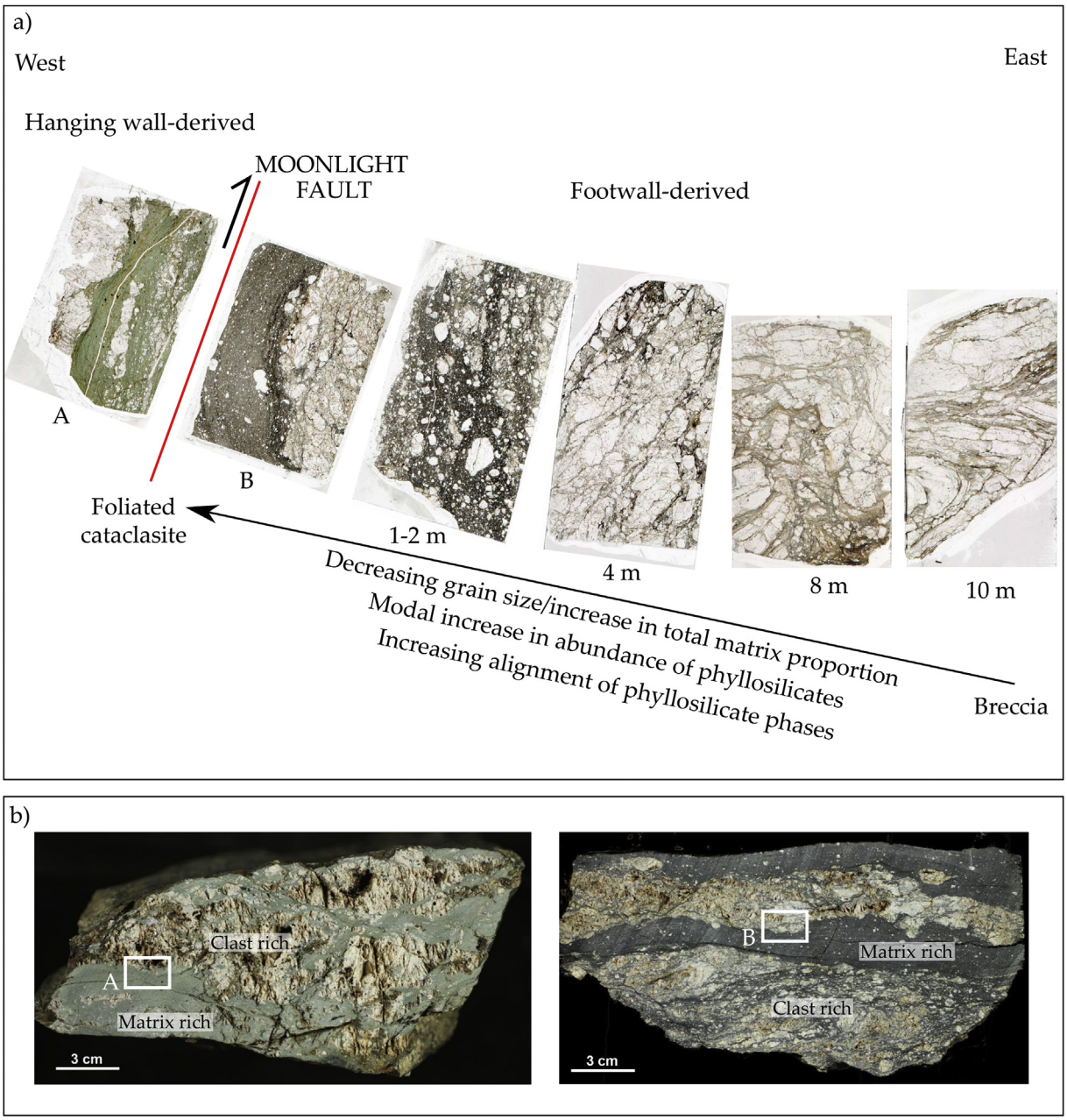

Fig. 9. Textural changes observed in fault rocks collected across the core of the Moonlight Fault Zone in the Matukituki Valley. a) Series of scanned thin sections from samples collected at distances of <10 m from the fault core illustrating the progression from intact footwall greyschist to breccia, cataclasite and foliated cataclasite. The fault core contains foliated cataclasites derived from the hanging-wall greenschists (A) and the footwall greyschists (B). b) Photographs of foliated cataclasites within the fault core illustrating the anastomosing and interconnected nature of the phyllosilicate-rich matrices. Clasts are dominated by quartz and albite. Green sample on the left is foliated cataclasite derived from the hanging-wall greenschists. Sample on the right is foliated cataclasite derived from footwall greyschists. (For interpretation of the references to colour in this figure legend, the reader is referred to the web version of this article.)

7. Discussion

7.1. Constraints on exhumation and offset

Host rocks of the MFZ contain a mineralogy (eg. albite, quartz, muscovite, chlorite, epidote, titanite) indicating peak metamorphism at chlorite-zone lower greenschist facies, which occurred at around 300 °C and 4–5 kbar (Mortimer, 2000). Exhumation of the west Otago area occurred due to regional uplift resulting from oblique transpression across the Australian-Pacific plate boundary that began at 5 ± 2 Ma (Norris et al., 1990). Uplift was greatest along the plate boundary (20–25 km) and decreased to the south-east (Cooper, 1980; Tippett and Kamp, 1993). Zircon fission track data retrieved from the basement rocks either side of the Moonlight Fault in the Matukituki Valley by Tippett and Kamp (1993) suggest that the area has been exhumed from around 9.5 ± 2.1 km depth in the last c. 5 Ma.

The Oligocene sedimentary sequences (Bobs Cove Beds) deposited during extensional movements along the MFZ had an estimated maximum thickness of 2–4 km (Norris et al., 1978; Norris and Carter, 1982), although they are now preserved only as fault-bound slivers in the footwall of the MFZ. This suggests that the

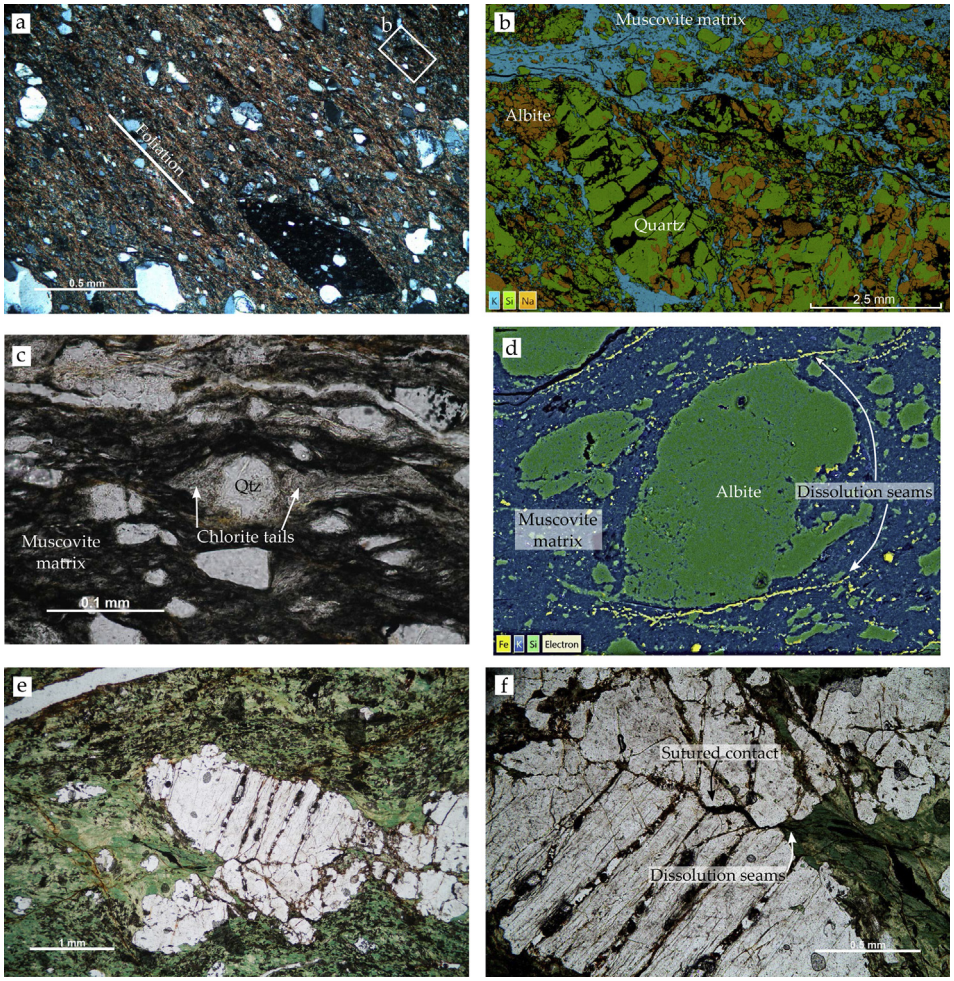

Fig. 10. Microstructures and deformation processes in the fault core. a,c,e and f are optical photomicrographs; b and d are SEM-EDS chemical maps showing the relative concentrations of various elements. a) Matrix-rich domain in the footwall-derived foliated cataclasites where the phyllosilicates form an interconnected network. The large dark clast at the bottom of the image is reworked cataclasite. b) Distribution of muscovite (rich in K) in the matrix-rich and clast-rich regions of the footwall-derived foliated cataclasites. Clasts consist of quartz (Si-rich) and albite (Na-rich). In the matrix-rich regions, muscovite forms an interconnected network surrounding clasts of quartz and albite. c) Authigenic chlorite forms tails around a quartz clast in the footwall-derived foliated cataclasites. d) Fe-rich dissolution seams in the matrix truncate the upper and lower edges of quartz and albite clasts. e) Chlorite (green) dominates in the matrix-rich regions of the hanging-wall-derived foliated cataclasites. Small black grains are mainly epidote. Quartz and albite clasts are highly fractured. f) Sutured contact between two albite grains with a concentration of opaque minerals defining a dissolution seam between clasts. The seam continues in to the surrounding chlorite-rich matrix. (For interpretation of the references to colour in this figure legend, the reader is referred to the web version of this article.)

basal Oligocene unconformity observed in several of the studied creek sections (Fig 3) cannot have been at more than c. 4 km depth before reverse reactivation of the MFZ. This constrains maximum uplift of the footwall to c. 4 km. The Oligocene sediments are not preserved in the hanging-wall of the MFZ to the north of Lake Wakatipu, suggesting that the hanging-wall has been exhumed from depths exceeding 2–4 km.

A structural thickness map of the Otago Schist based upon textural grade (Mortimer, 2003) suggests an apparent dip-slip reverse separation across the MFZ of c. 6–8 km in the Twelve Mile – Fan Creek region to the south, c. 5 km in the Moonlight – Stony Creek region and c. 3 km in the Matukituki Valley. The Matukituki Valley estimate is corroborated by Tippett and Kamp (1993) who suggested from zircon fission track data that reverse movement on the Moonlight Fault is unlikely to have exceeded 3 km in that area.

To summarise, best estimates of reverse offset along the Moonlight Fault Zone are in the range of 3–5 km, with offset possibly increasing south towards Lake Wakatipu. Exhumation is likely in the range of 4–10 km, increasing north towards the Alpine Fault. The creek sections we have studied therefore reveal structures and fault rock assemblages representative of a large-displacement, high-angle reverse fault that has been exhumed from mid- to upper-crustal depths.

7.2. Controls on fault-zone structure and implications for the mechanics of high-angle reverse faults

7.2.1. Hanging-wall damage and pseudotachylytes

Observations suggest that host rock lithology and anisotropy were the primary controls on the structure and fault rock assemblages that developed within the MFZ (Fig. 7). In the hanging-wall, pseudotachylyte networks formed in competent greenschists (Matukituki Valley, Stony Creek) and quartzofeldspathic gneiss (Moonlight Creek). Instead, where the hanging-wall contains fissile greyschists (Fan Creek, Twelve Mile Creek), fault-related damage occurred by the formation of breccia layers up to a few centimetres thick. Our results are in agreement with previous observations showing that pseudotachylyte mainly forms in competent crystalline rocks with low porosities that allow for the accumulation of sufficiently high levels of elastic strain energy required to generate frictional melt (Sibson, 1977; Sibson and Toy, 2006).

Hanging-wall damage in the MFZ occurs in a zone up to several hundreds of metres wide, in host rocks that contained a moderately- to steeply-west dipping schistosity at the time of reverse faulting. Of the pseudotachylyte fault veins observed in the Matukituki Valley, approximately 85% are subparallel to the foliation, suggesting that the foliation represented a strong anisotropy allowing for preferential failure. These observations are consistent with many other reports of natural pseudotachylyte (eg. Sibson, 1975; Swanson, 1988; Magloughlin and Spray, 1992). Summaries of experimental observations (Paterson and Wong, 2005; Bistacchi et al., 2012) indicate that the brittle shear strength of anisotropic rocks parallel to the foliation is approximately half of the brittle shear strength perpendicular to foliation, providing a mechanism to explain why pseudotachylyte commonly forms parallel to pre-existing anisotropy.

Pseudotachylyte fault veins in the hanging-wall are probably single-event structures with individual displacements of less than a few centimetres or, at most, a few tens of centimetres. Although the single-event origin is difficult to prove, no microstructural evidence was found for multiple melt-generating events along the same fault surface, although selvages of ultracataclasite along pseudotachylyte margins indicate that comminution preceded frictional melting (e.g.Swanson, 1992). Together with measurements showing that the density of pseudotachylyte fault veins in the hanging-wall is on the order of 0.1–10 fault veins per metre, the picture that emerges is of a wide (>500 m) hanging-wall damage zone riddled with foliation-parallel pseudotachylyte fault veins (Fig. 7). It appears that foliation surfaces were only activated once as small-displacement, melt-generating faults. One possible explanation is that foliation surfaces were "welded" together by the combined effects of comminution and cooling of the frictional melt. Once a pseudotachylyte had formed along a foliation surface, subsequent deformation events in the hanging-wall were preferentially accommodated on nearby foliation surfaces, ultimately leading to a wide hanging-wall network of pseudotachylytes that exploited the steeply west-dipping foliation. This model is similar to that proposed by Di Toro and Pennacchioni (2005) for the cataclasite- and pseudotachylyte-bearing fault networks in the Gole Larghe Fault Zone in Northern Italy. Total fault displacement of 1–2 km in the Gole Larghe Fault Zone was distributed across a network of cataclasites and pseudotachylytes up to 600 m wide (Smith et al., 2013) that exploited pre-existing cooling joints in the host rock tonalite (Di Toro and Pennacchioni, 2005). The low fault displacement:width ratio measured in the Gole Larghe Fault Zone was related to welding and hardening of fault surfaces by precipitation of syn-tectonic minerals in the matrix of the cataclasites, followed by the formation and cooling of pseudotachylytes (Di Toro and Pennacchioni, 2005).

7.2.2. Phyllosilicates, dissolution-precipitation and weakening in the fault core

Where greyschists are in contact with the main trace of the MFZ, a well-defined fault core is marked by a progressive sequence of breccias, cataclasites and foliated cataclasites that occupy a tabular layer up to 20 m thick (Fig. 7). This fault rock sequence was characterized in detail in the Matukituki Valley, but similar observations in the other creek sections (Fig. 3) indicate that such a fault rock sequence may typify the fault core over a strike length exceeding many tens of kilometres. This is significant because it suggests that the cataclasites and foliated cataclasites in the fault core are interconnected on scales ranging from the outcrop-scale up to the kilometric-scale. It follows that accumulation of reverse displacements on the MFZ was probably strongly influenced by the mechanical and hydrological properties of the cataclasites and foliated cataclasites (Holdsworth, 2004).

Microstructural evidence from the fault core sequence preserved in the Matukituki Valley indicates the cooperative activity of several deformation mechanisms. Initially, fracturing of the greyschists led to formation of random-fabric breccias. A likely consequence is that grain-scale dilatancy associated with brecciation triggered the formation of fluid pathways and the influx of fluids in to the fault core. In the higher-strain cataclasites and foliated cataclasites there is a notable increase in the modal abundance of phyllosilicate phases, which also became progressively aligned to define a new, steeply-west dipping foliation (Fig. 9). Quantitative XRD analysis indicates that foliated cataclasites derived from hanging-wall greenschists are dominated by chlorite, whereas footwall-derived foliated cataclasites are dominated by muscovite. In parallel with the increase in phyllosilicate content, microstructures including seams of relatively insoluble minerals and fibrous overgrowths of chlorite indicate that the foliated cataclasites deformed by dissolution – precipitation mechanisms that accompanied frictional sliding of phyllosilicate grains. Dissolution occurred at sites of high strain and produced features such as pressure solution seams and sutured/indented albite clasts. Precipitation occurred as fibrous chlorite overgrowths in areas such as the trailing edges of rigid albite and quartz clasts. Overall, the preserved fault rock sequence documents the progressive breakdown of a "load-bearing" framework (Handy, 1990) dominated by quartz and albite clasts to form an interconnected, anastomosing network of fine-grained phyllosilicates that dominate the inner portions of the fault core (Holdsworth, 2004; Jefferies et al., 2006a,b).

Several authors have inferred that fault rock fabric transitions such as that documented in the core of the MFZ (Fig. 9) can lead to significant long-term mineralogical weakening of fault zones as the frictional strength of phyllosilicate phases becomes dominant over the strength of framework silicates like quartz and albite (Wintsch et al., 1995; Imber et al., 2001; Jefferies et al., 2006a,b; Wallis et al., 2013; Wallis et al., 2015). Experiments on muscovite and chlorite (Scruggs and Tullis, 1998; Morrow et al., 2000; Brown et al., 2003; Kopf and Brown, 2003; Moore and Lockner, 2004; Niemeijer and Spiers, 2005; Mariani et al., 2006; Ikari et al., 2009; Van Diggelen et al., 2010; Behnsen and Faulkner, 2012; den Hartog et al., 2013) show that under a wide range of conditions the friction coefficients are in the range of $\mu = 0.312–0.619$ for muscovite and $\mu = 0.18–0.38$ for chlorite. Samples of natural gouge from the Alpine Fault, which contain modal contents of muscovite/illite and chlorite slightly lower than the foliated cataclasites from the MFZ, were experimentally deformed as foliated wafers by Boulton et al. (2012) and Barth et al. (2013) in a saturated state, at room temperature and effective normal stresses of 6–31 MPa. Under these conditions the frictional strength was $\mu = 0.28–0.37$. Because frictional strength can decrease with increasing gouge purity (Niemeijer and Spiers, 2005; den Hartog et al., 2013), samples of chlorite- and muscovite-rich foliated cataclasites from the MFZ may have lower values of frictional strength than those measured by Boulton et al. (2012) and Barth et al. (2013).

A wide phyllosilicate-rich fault core is also likely to represent a low-permeability barrier to migrating crustal fluids. Faulkner and Rutter (2001) report permeabilities in the range of 10^{-17} m^2 to 10^{-22} m^2 for muscovite/illite-rich and chlorite-rich gouges collected from the Carboneras Fault Zone in Spain, with the lowest values of permeability measured at high angles to the main fault rock foliation. More recently, Boulton et al. (2012) measured the permeability of foliated chlorite- and muscovite-bearing gouges collected from the Alpine Fault to be on the order of 3.10×10^{-20} m^2. In the MFZ, there is a lack of extensive vein networks in the fault core, the only exception being a series of metre-scale quartz veins in Fan Creek that taper upwards from the main fault trace in to the hanging-wall.

This suggests that fluid overpressures were not widely developed in the fault core or that evidence of fluid overpressure (e.g. vein networks) was destroyed by subsequent fault movements. However, it is noteworthy that pseudotachylytes – typically associated with faulting in relatively dry and strong crustal rocks (Sibson and Toy, 2006) – are only found in the hanging-wall of the MFZ, imparting a distinct asymmetry to the overall structure of the fault zone. Although this could have a number of explanations, one possibility is that the fault core acted as an efficient hydrological barrier, resulting in a relatively hydrous footwall and fault core but a relatively dry hanging-wall. Circumstantial evidence to support this interpretation comes from the distribution of Moonlight-age (Miocene) gold mineralization and associated hydrothermal quartz-ankerite alteration in the Shotover-Macetown mineralized area between Queenstown and Wanaka (Fig. 2c). In this area, the principal mineralized zones are found in mesoscopic faults, veins and folds that formed during steep reverse movements on the nearby MFZ (Craw et al., 2006). The mineralized zones are restricted to the footwall of the MFZ in an area of fissile, hydrothermally altered schist, which led Craw et al. (2006) to suggest that the "..hanging-wall, combined with the cataclasites of the fault zone itself, have formed an impermeable barrier to passage of hydrothermal fluids."

Our field observations suggest that the frictional properties of phyllosilicate-rich fault rocks potentially influence the mechanical behaviour of basin-scale reverse faults. In the two-dimensional reactivation models of Sibson (1985) a reverse fault dipping at >60° and possessing a friction coefficient, μ, of 0.6 can only be reactivated in an "Andersonian" stress state (with vertical σ_3) if fluid overpressure exceeds σ_3. However, in the case that the friction coefficient parallel to the steeply-dipping fault is μ<0.6, the requirement of fluid overpressure as a necessary condition for reverse-fault reactivation is reduced (Massironi et al., 2011; Bistacchi et al., 2012). For example, considering a representative friction coefficient for chlorite of $\mu = 0.3$ (see references above), a reverse fault dipping at 60° will be reactivated in preference to the formation of new, optimally-oriented thrusts at hydrostatic fluid pressure levels (i.e. λ ~0.4).

Compilations of reverse-fault dip estimates from moderate to large intracontinental earthquakes show a cluster of data at dip values of 45–55° (Sibson and Xie, 1998; Collettini and Sibson, 2001). An important implication is that nearly all (perhaps all) active, large-displacement reverse faults are due to compressional inversion of normal faults in areas undergoing tectonic inversion (Sibson and Xie, 1998). If this is the case, then mature phyllosilicate-rich fault rocks may be present in the fault core region from the earliest stages of high-angle reverse faulting, being an inherited feature from the older basin-bounding normal faults (Massironi et al., 2011). It therefore seems probable in the case of basin-scale reverse faults that the effects of a low-permeability, phyllosilicate-rich fault core will lead to both episodic fluid overpressuring and long-term mineralogical weakening that combine to facilitate slip on high-angle reverse faults.

8. Conclusions

The Moonlight Fault Zone was a large basin-bounding normal fault that reactivated as a high-angle reverse fault. Exposures of the steeply-dipping (65°–75°) fault zone in basement rocks were exhumed from c. 4–10 km depth. The structure of the Moonlight Fault Zone at these depths was controlled to a large degree by the lithology and mechanical anisotropy of the schistose host rocks. Networks of steeply-dipping pseudotachylytes formed in the hanging-wall in regions where competent greenschists or quartzofeldspathic schists and gneisses dominate, while layer-parallel breccias formed in more fissile greyschists. The core of the Moonlight Fault Zone contains a c. 20 m thick sequence of breccias, cataclasites and foliated cataclasites rich in chlorite and muscovite that deformed by a combination of cataclasis, frictional sliding and dissolution-precipitation. Our observations of a wide and phyllosilicate-rich fault core suggest that relatively low frictional strength is a plausible mechanism to facilitate high-angle reverse slip, and should be considered in mechanical models together with other potential weakening mechanisms including high fluid pressures and stress rotation. The restriction of pseudotachylyte networks to the hanging-wall of the Moonlight Fault Zone also suggests that the fault core acted as an efficient hydrological barrier.

Acknowledgements

This work was supported by the Marsden Fund Council (project UOO1417 to Smith) administered by the Royal Society of New Zealand. Simon Alder acknowledges additional support from the American Association of Petroleum Geologists Foundation Grants-in-Aid Program and the Hutton Fund of the Royal Society of New Zealand. Kat Lilly provided assistance with the FEG-SEM in the Otago Centre for Electron Microscopy (OCEM) at the University of Otago. Mark Raven and Peter Self of CSIRO carried out the quantitative XRD analysis. Brent Pooley prepared excellent thin sections. Tristan Menzies and Chris Tulley contributed data on the Fan Creek section during their BSc (Hons) projects in Otago. Andrea Bistacchi and Dan Faulkner provided thoughtful reviews that helped to clarify many aspects of the manuscript.

References

Barber, A., Craw, D., 2002. Lithology, geochemistry, and structure of Moke Creek sulphide deposit host rocks, Otago Schist, New Zealand. New Z. J. Geol. Geophys. 45, 193–205.
Barry, J., 1966. Structural Analysis in the Middle Shotover Valley. University of Otago, Northwest Otago.
Barth, N.C., Boulton, C., Carpenter, B.M., Batt, G.E., Toy, V.G., 2013. Slip localization on the southern Alpine Fault, New Zealand. Tectonics 32, 620–640.
Behnsen, J., Faulkner, D.R., 2012. The effect of mineralogy and effective normal stress on frictional strength of sheet silicates. J. Struct. Geol. 42, 49–61.
Bishop, D.J., Buchanan, P.G., 1995. Development of Structurally Inverted Basins: a Case Study from the West Coast, South Island, New Zealand. Geological Society, London, pp. 549–585. Special Publications 88.
Bistacchi, A., Massironi, M., Menegon, L., Bolognesi, F., Donghi, V., 2012. On the nucleation of non-Andersonian faults along phyllosilicate-rich mylonite belts. In: Healy, D., Butler, R.W.H., Shipton, Z.K., Sibson, R.H. (Eds.), Faulting, Fracturing and Igneous Intrusion in the Earth's Crust. Geological Society of London, London, pp. 185–199. Special Publications.
Boulton, C., Carpenter, B., Toy, V., Marone, C., 2012. Physical properties of surface outcrop cataclastic fault rocks, Alpine Fault, New Zealand. Geochem. Geophys. Geosys. 13.
Brown, K.M., Kopf, A., Underwood, M.B., Weinberger, J.L., 2003. Compositional and fluid pressure controls on the state of stress on the Nankai subduction thrust: a weak plate boundary. Earth Planet. Sci. Lett. 214, 589–603.
Collettini, C., Niemeijer, A., Viti, C., Marone, C., 2009. Fault zone fabric and fault weakness. Nature 462, 907–910.
Collettini, C., Sibson, R.H., 2001. Normal faults, normal friction? Geology 29, 927–930.
Cooper, A.F., 1980. Retrograde alteration of chromian kyanite in metachert and amphibolite whiteschist from the Southern Alps, New Zealand, with implications for uplift on the Alpine Fault. Contrib. Miner. Pet. 75, 153–164.
Cox, S.F., 1995. Faulting processes at high fluid pressures - an example of fault valve behavior from the Wattle Gully fault, Victoria, Australia. J. Geophys. Res. Solid Earth 100, 12841–12859.
Craw, D., 1985. Structure of schist in the Mt Aspiring region, Northwestern Otago, New-Zealand. New Z. J. Geol. Geophys. 28, 55–75.
Craw, D., Begbie, M., MacKenzie, D., 2006. Structural controls on Tertiary orogenic gold mineralization during initiation of a mountain belt, New Zealand. Min. Depos. 41, 645–659.
den Hartog, S.A.M., Niemeijer, A.R., Spiers, C.J., 2013. Friction on subduction megathrust faults: beyond the illite–muscovite transition. Earth Planet. Sci. Lett. 373, 8–19.
Di Toro, G., Pennacchioni, G., 2005. Fault plane processes and mesoscopic structure of a strong-type seismogenic fault in tonalites (Adamello batholith, Southern

Alps). Tectonophysics 402, 55–80.
Doré, A., Lundin, E., 1996. Cenozoic compressional structures on the NE Atlantic margin; nature, origin and potential significance for hydrocarbon exploration. Pet. Geosci. 2, 299–311.
Faulkner, D.R., Rutter, E.H., 2001. Can the maintenance of overpressured fluids in large strike-slip fault zones explain their apparent weakness? Geology 29, 503–506.
Faulkner, D.R., Mitchell, T.M., Healy, D., Heap, M.J., 2006. Slip on 'weak' faults by the rotation of regional stress in the fracture damage zone. Nature 444, 922–925.
Fraser, A., Gawthorpe, R., 1990. Tectono-stratigraphic Development and Hydrocarbon Habitat of the Carboniferous in Northern England. Geological Society, London, pp. 49–86. Special Publications 55.
Ghisetti, F., Sibson, R., 2006. Accommodation of compressional inversion in northwestern South Island (New Zealand): old faults versus new? J. Struct. Geol. 28, 1994–2010.
Ghisetti, F., Sibson, R., 2012. Compressional reactivation of E–W inherited normal faults in the area of the 2010–2011 Canterbury earthquake sequence. New Z. J. Geol. Geophys. 55, 177–184.
Ghisetti, F., Sibson, R.H., Hamling, I., 2016. Deformed Neogene basins, active faulting and topography in Westland: distributed crustal mobility west of the Alpine Fault transpressive plate boundary (South Island, New Zealand). Tectonophysics. http://dx.doi.org/10.1016/j.tecto.2016.03.024 (in press).
Grindley, G.W., 1963. Structure of the alpine schists of south Westland, southern Alps, New Zealand. New Z. J. Geol. Geophys. 6, 872–930.
Hacket, J.R., 1864. Report on Limestone at Lake Wakatipu (Otago Provincial Government Gazette).
Handy, M.R., 1990. The solid-state flow of polymineralic rocks. J. Geophys. Res. Solid Earth Planets 95, 8647–8661.
Harding, T.P., Lowell, J.D., 1979. Structural styles, their plate-tectonic habitats, and hydrocarbon traps in petroleum provinces. AAPG Bull. 63, 1016–1058.
Holdsworth, R.E., 2004. Weak faults–rotten cores. Science 303, 181–182.
Hutton, C.O., 1939. The Bob's Cove beds and the Moonlight thrust-fault. Trans. Proc. R. Soc. N. Z. 69, 73–88.
Ikari, M.J., Saffer, D.M., Marone, C., 2009. Frictional and hydrologic properties of clay-rich fault gouge. J. Geophys. Res. Solid Earth 114 (n/a-n/a).
Imber, J., Holdsworth, R.E., Butler, C.A., Strachan, R.A., 2001. A reappraisal of the Sibson-Scholz fault zone model: the nature of the frictional to viscous ("brittle-ductile") transition along a long-lived, crustal-scale fault, Outer Hebrides, Scotland. Tectonics 20, 601–624.
Jefferies, S.P., Holdsworth, R.E., Shimamoto, T., Takagi, H., Lloyd, G.E., Spiers, C.J., 2006a. Origin and mechanical significance of foliated cataclastic rocks in the cores of crustal-scale faults: examples from the Median Tectonic Line, Japan. J. Geophys. Res. Solid Earth 111 (Online Only).
Jefferies, S.P., Holdsworth, R.E., Wibberley, C.A.J., Shimamoto, T., Spiers, C.J., Niemeijer, A.R., Lloyd, G.E., 2006b. The nature and importance of phyllonite development in crustal-scale fault cores: an example from the Median Tectonic Line, Japan. J. Struct. Geol. 28, 220–235.
Kopf, A., Brown, K.M., 2003. Friction experiments on saturated sediments and their implications for the stress state of the Nankai and Barbados subduction thrusts. Mar. Geol. 202, 193–210.
Lin, A., 2008. Fossil Earthquakes: the Formation and Preservation of Pseudotachylytes. Springer Berlin Heidelberg, Berlin.
Litchfield, N.J., 2001. The Titri Fault System: quaternary-active faults near the leading edge of the Otago reverse fault province. New Z. J. Geol. Geophys. 44, 517–534.
Logan, J.M., Friedman, M., Higgs, N., Dengo, C., Shimamoto, T., 1979. Experimental studies of simulated gouge and their application to studies of natural fault zones. In: U.S. Geological Survey Open-File Report, Proceedings of Conference VIII on analysis of actual fault zones in bedrock, pp. 305–343.
Magloughlin, J.F., Spray, J.G., 1992. Frictional melting processes and products in geological materials: introduction and discussion. Tectonophysics 204, 197–204.
Mariani, E., Brodie, K.H., Rutter, E.H., 2006. Experimental deformation of muscovite shear zones at high temperatures under hydrothermal conditions and the strength of phyllosilicate-bearing faults in nature. J. Struct. Geol. 28, 1569–1587.
Massironi, M., Bistacchi, A., Menegon, L., 2011. Misoriented faults in exhumed metamorphic complexes: rule or exception? Earth Planet. Sci. Lett. 307, 233–239.
McClay, K., 1995. The Geometries and Kinematics of Inverted Fault Systems: a Review of Analogue Model Studies. Geological Society, London, pp. 97–118. Special Publications 88.
McKay, A., 1881. The District West and North of Lake Wakatipu. NZ. Geological Survey Reports of Geological Explorations 1879-1880, Wellington.
Mescua, J.F., Giambiagi, L.B., 2012. Fault inversion vs. new thrust generation: a case study in the Malargüe fold-and-thrust belt, Andes of Argentina. J. Struct. Geol. 35, 51–63.
Moore, D.E., Lockner, D.A., 2004. Crystallographic controls on the frictional behavior of dry and water-saturated sheet structure minerals. J. Geophys. Res. Solid Earth 109 (Online Only).
Morrow, C.A., Moore, D.E., Lockner, D.A., 2000. The effect of mineral bond strength and adsorbed water on fault gouge frictional strength. Geophys. Res. Lett. 27, 815–818.
Mortimer, N., 2000. Metamorphic discontinuities in orogenic belts: example of the garnet–biotite–albite zone in the Otago Schist, New Zealand. Int. J. Earth Sci. 89, 295–306.
Mortimer, N., 2003. A provisional structural thickness map of the Otago Schist, New Zealand. Am. J. Sci. 303, 603–621.
Mortimer, N., Davey, F.J., Melhuish, A., Yu, J., Godfrey, N.J., 2002. Geological interpretation of a deep seismic reflection profile across the Eastern Province and Median Batholith, New Zealand: crustal architecture of an extended Phanerozoic convergent orogen. New Z. J. Geol. Geophys. 45, 349–363.
Mortimer, N., Tulloch, A., Spark, R., Walker, N., Ladley, E., Allibone, A., Kimbrough, D., 1999. Overview of the median batholith, New Zealand: a new interpretation of the geology of the median tectonic zone and adjacent rocks. J. Afr. Earth Sci. 29, 257–268.
Niemeijer, A.R., Spiers, C.J., 2005. Influence of Phyllosilicates on Fault Strength in the Brittle-ductile Transition: Insights from Rock Analogue Experiments. Geological Society, London, pp. 303–327. Special Publications 245.
Norris, R.J., Carter, R.M., 1982. Fault-bounded blocks and their role in localising sedimentation and deformation adjacent to the alpine fault, southern New Zealand. Tectonophysics 87, 11–23.
Norris, R.J., Carter, R.M., Turnbull, I.M., 1978. Cainozoic sedimentation in basins adjacent to a major continental transform boundary in southern New Zealand. J. Geol. Soc. 135, 191–205.
Norris, R.J., Koons, P.O., Cooper, A.F., 1990. Australasian tectonics the obliquely-convergent plate boundary in the South Island of New Zealand: implications for ancient collision zones. J. Struct. Geol. 12, 715–725.
Norris, R.J., Koons, P.O., Cooper, A.F., 1990b. The obliquely-convergent plate boundary in the South Island of New Zealand: implications for ancient collision zones. J. Struct. Geol. 12, 715–725.
Park, J., 1909. The Geology of the Queenstown Subdivision. Bulletin N.Z. Geological Survey 7.
Paterson, M.S., Wong, T.F., 2005. Experimental Rock Deformation: the Brittle Field, 2 ed. Springer.
Rattenbury, M.S., Jongens, R., Cox, S.C., 2010. Geology of the Wakatipu Area. Institute of Geological & Nuclear Sciences Ltd, Lower Hutt, New Zealand.
Reilly, C., Nicol, A., Walsh, J.J., Seebeck, H., 2015. Evolution of faulting and plate boundary deformation in the Southern Taranaki Basin, New Zealand. Tectonophysics 651, 1–18.
Reyners, M., Ingham, C.E., Ferris, B.G., 1983. Microseismicity of the upper Clutha valley, South Island, New Zealand. New Z. J. Geol. Geophys. 26, 1–6.
Rice, J.R., 1992. Fault stress states, pore pressure distributions, and the weakness of the San Andreas fault. In: Evans, B., Wong, T.F. (Eds.), Fault Mechanics and Transport Properties of Rocks. Academic Press, London, pp. 475–503.
Scholz, C.H., Rynn, J.M.W., Weed, R.W., Frohlich, C., 1973. Detailed seismicity of the Alpine Fault zone and Fiordland region, New Zealand. Geol. Soc. Am. Bull. 84, 3297–3316.
Scott, J., 2013. A review of the location and significance of the boundary between the Western Province and Eastern Province, New Zealand. New Z. J. Geol. Geophys. 56, 276–293.
Scruggs, V.J., Tullis, T.E., 1998. Correlation between velocity dependence of friction and strain localization in large displacement experiments on feldspar, muscovite and biotite gouge. Tectonophysics 295, 15–40.
Sibson, R.H., 1975. Generation of pseudotachylyte by ancient seismic faulting. Geophys. J. Int. 43, 775–794.
Sibson, R.H., 1977. Fault rocks and fault mechanisms. J. Geol. Soc. 133, 191–213.
Sibson, R.H., 1985. A Note on Fault Reactivation. J. Struct. Geol. 7, 751–754.
Sibson, R.H., 1990. Rupture nucleation on unfavorably oriented faults. Bull. Seismol. Soc. Am. 80, 1580–1604.
Sibson, R.H., 1995. Selective Fault Reactivation during Basin Inversion: Potential for Fluid Redistribution through Fault-valve Action. Geological Society, London, pp. 3–19. Special Publications 88.
Sibson, R.H., 2007. An episode of fault-valve behaviour during compressional inversion? — the 2004 MJ6.8 Mid-Niigata Prefecture, Japan, earthquake sequence. Earth Planet. Sci. Lett. 257, 188–199.
Sibson, R.H., 2009. Rupturing in overpressured crust during compressional inversion—the case from NE Honshu, Japan. Tectonophysics 473, 404–416.
Sibson, R.H., Robert, F., Poulsen, K.H., 1988. High-angle reverse faults, fluid-pressure cycling, and mesothermal gold-quartz deposits. Geology 16, 551–555.
Sibson, R.H., Toy, V.G., 2006. The habitat of fault-generated pseudotachylyte: presence vs. absence of friction-melt. In: Abercrombie, R., McGarr, A., Di Toro, G., Kanamori, H. (Eds.), Earthquakes: Radiated Energy and the Physics of Faulting. Amer Geophysical Union, Washington, pp. 153–166.
Sibson, R.H., Xie, G., 1998. Dip range for intracontinental reverse fault ruptures: truth not stranger than friction? Bull. Seismol. Soc. Am. 88, 1014–1022.
Smith, S.A.F., Bistacchi, A., Mitchell, T.M., Mittempergher, S., Di Toro, G., 2013. The structure of an exhumed intraplate seismogenic fault in crystalline basement. Tectonophysics 599, 29–44.
Smith, S.A.F., Faulkner, D.R., 2010. Laboratory measurements of the frictional properties of the Zuccale low-angle normal fault, Elba Island, Italy. J. Geophys. Res. Solid Earth 115.
Spray, J.G., 1995. Pseudotachylyte controversy: fact or friction? Geology 23, 1119–1122.
Swanson, M.T., 1988. Pseudotachylyte-bearing strike-slip duplex structures in the Fort Foster brittle zone, S. Maine. J. Struct. Geol. 10, 813–828.
Swanson, M.T., 1992. Fault structure, wear mechanisms and rupture processes in pseudotachylyte generation. Tectonophysics 204, 223–242.
Tippett, J.M., Kamp, P.J.J., 1993. The role of faulting in rock uplift in the Southern Alps, New Zealand. New Z. J. Geol. Geophys. 36, 497–504.
Townend, J., Sherburn, S., Arnold, R., Boese, C., Woods, L., 2012. Three-dimensional

variations in present-day tectonic stress along the Australia–Pacific plate boundary in New Zealand. Earth Planet. Sci. Lett. 353–354, 47–59.
Turnbull, I.M., 1969. Stratigraphy, Structure and Metamorphism in the Bobs Cove: Moke Creek: Queenstown Area, Lake Wakatipu. Geology. University of Otago.
Turnbull, I.M., Barry, J.M., Carter, R.M., Norris, R.J., 1975. The Bobs Cove beds and their relationship to the Moonlight Fault zone. J. R. Soc. N. Z. 5, 355–394.
Turner, J.P., Williams, G.A., 2004. Sedimentary basin inversion and intra-plate shortening. Earth Sci. Rev. 65, 277–304.
Van Diggelen, E.W.E., De Bresser, J.H.P., Peach, C.J., Spiers, C.J., 2010. High shear strain behaviour of synthetic muscovite fault gouges under hydrothermal conditions. J. Struct. Geol. 32, 1685–1700.
Wallis, D., Lloyd, G.E., Phillips, R.J., Parsons, A.J., Walshaw, R.D., 2015. Low effective fault strength due to frictional-viscous flow in phyllonites, Karakoram Fault Zone, NW India. J. Struct. Geol. 77, 45–61.
Wallis, D., Phillips, R.J., Lloyd, G.E., 2013. fault weakening across the frictional-viscous transition zone, Karakoram fault zone, NW Himalaya. Tectonics 32, 1227–1246.
Warren-Smith, E., Lamb, S., Stern, T.A., Chamberlain, C.J., 2015. What controls slip directions of diffuse microseismicity in a zone of continental transpression, South Island, New Zealand?. In: Poster Session Presented at the Meeting of the American Geophysical Union Fall Meeting, San Francisco. Presentation Number T43C-3032.
Wintsch, R.P., Christoffersen, R., Kronenberg, A.K., 1995. Fluid-rock reaction weakening of fault zones. J. Geophys. Res. Solid Earth 100, 13021–13032.